Durable nanofibrous matrices augmented with hydrotalcite-like compounds for cutaneous regeneration of burn wounds

Vimala Devi, Mohan; Sobhana, S.S. Liji; Shiny, Punalur John; Ramanathan, Giriprasath; Grace Felciya, Sekar Jeyakumar; Poornima, Velswamy; Thennarasu, Sathiah; Fardim, Pedro; Sivagnanam, Uma Tiruchirapalli

Published in:
Applied Clay Science

DOI:
10.1016/j.clay.2020.105476

Published: 01/02/2020

Document Version
Accepted author manuscript

Document License
CC BY-NC-ND

Elsevier Editorial System(tm) for Applied Clay Science

Manuscript Draft

Manuscript Number: CLAY13714R2

Title: Durable nanofibrous matrices augmented with hydrotalcite-like compounds for cutaneous regeneration of burn wounds

Article Type: Research Paper

Keywords: Burns; Wound Healing; Nanofibrous matrix; LDH; Biocompatibility; In vivo study

Corresponding Author: Dr. Uma Tiruchirapalli Sivagnanam, PhD

Corresponding Author's Institution: CLRI

First Author: Vimala Devi Mohan

Order of Authors: Vimala Devi Mohan; Liji Sobhana S. S; Shiny Punalur John; Giriprasath Ramanathan; Grace Felciya Sekar Jeyakumar; Poornima Velswamy; Sathiah Thennarasu; Pedro Fardim; Uma Tiruchirapalli Sivagnanam, PhD

Abstract: Electrospinning of Gelatin (G) and Poly-3-hydroxybutyric acid (P) incorporated with anionic drug (AgSD) loaded hydrotalcite (L) (L-AgSD) is carried out to fabricate a nanofibrous scaffold which would recreate the native extracellular matrix suitable for cutaneous regeneration. The L-AgSD complex was augmented into electrospun nanofibers of diameter 100-140 nm. The physiochemical (XRD, FTIR), morphological (SEM), mechanical (tensile strength) and biological (in vitro and in vivo) properties of the developed wound construct were studied. Antimicrobial studies reveal the potential activity against microbial infection. Studies on drug release kinetics demonstrate a controlled drug release of 86% in 72 hours. In vitro biocompatibility studies using NIH 3T3 fibroblast cell line showed excellent cell adhesion and cell proliferation indicating the biocompatible nature of the scaffold. The matrix accelerated wound healing on Pseudomonas infected burn wound induced on rat models. The tailored matrix is promising as an impending nanohybrid construct for burn wound injuries with controlled drug release and antibacterial activity.

Response to Reviewers: Response to reviewers' comments
Title: Durable nanofibrous matrices augmented with hydrotalcite-like compounds for
cutaneous regeneration of burn wounds

Ref.: Manuscript.: CLAY 13714R1

We thank all the reviewers for their valuable comments and their suggestion. As per the reviewer's suggestions the manuscript was rewritten. The corrections and changes were carried out in the main manuscript. We also addressed all the reviewers' comments and prepared a detailed response to reviewer and all the changes were given in red colour in the revised manuscript.

Reviewer #2: The submitted manuscript was improved by the authors and deserve publication. Only minor suggestions are addressed:

Q1. Line 53: Modification in the sentence "Owing to these interesting properties, the current study proposes TO IMMOBILIZE A DRUG ON THE SURFACES OF LDH PARTICLES".

As suggested by the reviewer the modification in the sentence was carried out and the changes have been carried out accordingly in the revised manuscript.

Q2. Line 175: Suppression of the sentence "It was also observed that the arrangement of Mg2+ and Al3+ cations in the brucite layers was clearly distinct which has made the material more crystalline".

As suggested by the reviewer the suppression of the sentence was made and the same has been carried out accordingly in the revised manuscript.

Q3. Line 207: Modification in the sentence "The mass loss of this region was also attributed to the loss of WATER and CO2 through slow decomposition of the inorganic phases after the disruption of the hydrotalcite.

As suggested by the reviewer the modification in the sentence was carried out and the changes have been carried out accordingly in the revised manuscript.

Q4. Line 249: the authors claim that "… no characteristic reflections were observed both in LDH loaded and nanohybrid loaded polymeric matrix indicating that LDH has lost its basal periodicity in the polymeric network". Both the drug and the polymer present higher crystallinity than LDH, which can avoid the visualization of LDH peaks. In our opinion, this is more plausible than the "loss of basal periodicity" in the soft experimental conditions

As suggested by the reviewer the plausible sentence was removed and the same has been carried out accordingly in the revised manuscript.

Research Data Related to this Submission

There are no linked research data sets for this submission. The following reason is given:
The data that has been used is confidential

Response to reviewers' comments

Title: ***Durable nanofibrous matrices augmented with hydrotalcite-like compounds for cutaneous regeneration of burn wounds***

Ref.: Manuscript.: **CLAY 13714R1**

We thank all the reviewers for their valuable comments and their suggestion. As per the reviewer's suggestions the manuscript was rewritten. The corrections and changes were carried out in the main manuscript. We also addressed all the reviewers' comments and prepared a detailed response to reviewer and all the changes were given in red colour in the revised manuscript.

Reviewer #2: The submitted manuscript was improved by the authors and deserve publication. Only minor suggestions are addressed:

Q1. Line 53: Modification in the sentence "Owing to these interesting properties, the current study proposes TO IMMOBILIZE A DRUG ON THE SURFACES OF LDH PARTICLES".

As suggested by the reviewer the modification in the sentence was carried out and the changes have been carried out accordingly in the revised manuscript.

Q2. Line 175: Suppression of the sentence "It was also observed that the arrangement of Mg2+ and Al3+ cations in the brucite layers was clearly distinct which has made the material more crystalline".

As suggested by the reviewer the suppression of the sentence was made and the same has been carried out accordingly in the revised manuscript.

Q3. Line 207: Modification in the sentence "The mass loss of this region was also attributed to the loss of WATER and CO2 through slow decomposition of the inorganic phases after the disruption of the hydrotalcite.

As suggested by the reviewer the modification in the sentence was carried out and the changes have been carried out accordingly in the revised manuscript.

Q4. Line 249: the authors claim that "… no characteristic reflections were observed both in LDH loaded and nanohybrid loaded polymeric matrix indicating that LDH has lost its basal periodicity in the polymeric network". Both the drug and the polymer present higher crystallinity than LDH, which can avoid the visualization of LDH peaks. In our opinion, this is more plausible than the "loss of basal periodicity" in the soft experimental conditions

As suggested by the reviewer the plausible sentence was removed and the same has been carried out accordingly in the revised manuscript.

Durable nanofibrous matrices augmented with hydrotalcite-like compounds for cutaneous regeneration of burn wounds

Vimala Devi Mohan[a], Liji Sobhana S. S.[c], Punalur John Shiny[a], Giriprasath Ramanathan[a,d], Grace Felciya Sekar Jeyakumar[a], Velswamy Poornima[a], Sathiah Thennarasu[b], Pedro Fardim[c,d,*], Uma Tiruchirapalli Sivagnanam[a,*]

[a]*Biological Materials Laboratory, CSIR-Central Leather Research Institute (CLRI), Adyar, Chennai, India*

[b]*Organic Chemistry Division, CSIR-Central Leather Research Institute (CLRI), Adyar, Chennai, India*

[c]*Laboratory of Fiber and Cellulose Technology, Abo Akademi University, Porthansgatan 3, FI-20500 Abo, Finland*

[d]*Chemical Engineering for Health & Care, Bio&Chemical Systems Technology, Reactor Engineering and Safety, Department of Chemical Engineering, KU Leuven, Celestijnenlaan 200F bus 2424, B-3001 Leuven, Belgium*

*** Corresponding authors email addresses:**

Dr. Uma Tiruchirapalli Sivagnanam (suma67@gmail.com),

Prof. Pedro Fardim (pfardim@abo.fi; pedro.fardim@kuleuven.be**)**

1. Introduction

Skin, the major organ of our body, functions to regulate the body temperature and protects us from external harmful factors. The chances of microbial infection and its associated risks are high in a damaged skin. This is inevitable to promote healing and reduce infection. Current challenges in wound care management include inadequate delivery of drug, poor contact between drug and the wound and irregular deposition of antimicrobial agents at the wound site. However, these limitations are addressed with the development of wound dressings, which can be applied as a protective cover over the injured site (Martin et al., 2013).

The development of wound dressing material began with the need of a physical barrier to prevent microbial infection and accelerate healing. The characteristic features of wound dressing material include absorption of wound exudates, inhibit microbial entry at wound site and enhance the aesthetics of skin. Previous studies clearly exhibits the various forms of dressings available in the market such as sponges (Dai et al., 2009), hydrogels (Ouyang et al., 2018), foams (Timmers et al., 2008) and films (O'Brien, 2011), which primarily contains hydrocolloids, alginates and composites. In addition, two-dimensional nanofibrous matrix are extensively preferred due to its high surface to volume ratio, oxygen permeability and biocompatibility (Garg et al., 2012). Nanofibrous matrix are yet another form of film-based dressing that mimic the function of natural extracellular matrix and serve as a suitable environment for cell attachment and proliferation (Smith and Ma, 2004; Unnithan et al., 2012). The current work explores the possibility of constructing a nanofibrous matrix with dual action of antimicrobial activity followed by wound healing through a drug propelled carrier system.

The use of layered double hydroxides (LDH) as a drug carrier, apart from its conventional use as catalysts, adsorbents, and environmental remediation materials has earned the interest of

47 scientists (Williams et al., 2006; Qiu and Hou, 2009; Jin et al., 2010; L. Sobhana et al., 2016; Liji
48 et al., 2016; S. S. L. Sobhana et al., 2016; Sobhana et al., 2017). As the name suggests, they are a
49 class of ionic lamellar compounds that are made of unique positively charged brucite-like layers
50 in which partial substitution of the divalent cations with trivalent ions give rise to positively
51 charged sheets counter balanced by anionic species. Several reports have documented the
52 efficacy of these hydrotalcite-like materials as carrier molecules (Shafiei et al., 2015; Ge et al.,
53 2016). Owing to these interesting properties, the current study proposes to immobilize a drug on
54 the surfaces of LDH particles. Many therapeutic molecules such as peptides, proteins and natural
55 organic molecules are negatively charged at neutral to near neutral pH values. Hence, they tend
56 to interact strongly with materials like LDH having positive charges. Thus, the drug carrying
57 ability of LDH can be extrapolated to wide range of drugs for medical applications.
58 Several antiseptic agents such as povidone-iodine, alcohol, chlorhexidine and honey are topically
59 used for the treatment of burn wounds (Andreu et al., 2015). Burn wounds are prone to bacterial
60 growth and infection (Jahromi et al., 2018). Silver-based dressing material still seems to be the
61 finest of choice for treating burn wound injuries and infections (Shanmugasundaram et al., 2009;
62 Heo et al., 2013; Shao et al., 2017). However, the bioavailability of the drug delivered through
63 cream based formulation is very low due to wash out with the exudates and lower absorption
64 resulting in frequent dressing changes that would traumatize the new epithelial surface resulting
65 in delayed wound healing (Sano et al., 1982).
66 The conventional methods used for the fabrication of matrix including that of phase separation
67 (Budyanto et al., 2009), extrusion (Kim et al., 2014), gas foaming (Jiang et al., 2015) and
68 template synthesis (Martín et al., 2012) suffer certain drawbacks such as use of only compatible
69 polymers, stability concerns on drug and polymer, poor pore interconnectivity, need for post-

synthesis process to remove the templates, etc. In order to overcome these drawbacks, an attempt was made to fabricate the nanofibrous matrix by electrospinning. The process of electrospinning offers various advantages such as ease of operation using wide range of polymers, cost-effective and yields nanofibers of high surface to volume ratio (Nagiah et al., 2013b).

In the present study, AgSD loaded LDH has been electrospun along with polymers to yield a therapeutic hybrid matrix. Nonetheless, the soluble form of silver is biologically active against microbes. Moreover, the AgSD dissociates in solution to form cationic silver ions and anionic sulfadiazine molecules to impart antibacterial property at the wound site. Gelatin (G), the renewable bio-protein was chosen due to its excellent biocompatibility, and adhesiveness (Nagiah et al., 2013a, 2013b; Rathore et al., 2016) However, gelatin as such cannot be electrospun due to its poor fiber-forming ability and mechanical stability. Hence, it has to be often blended with other polymers to obtain nanofiber through electrospinning (Fallah et al., 2016). Herein, Poly-3-hydroxybutyric acid (P), a biodegradable common metabolite present in all higher living organisms, which proves its non-toxicity was chosen for the fabrication of the scaffold (Matrix) (Nagiah et al., 2013b).

Furthermore, an attempt was made to deliver AgSD in a controlled fashion on the target site with the help of the fabricated carrier material, LDH. Moreover, the knowledge from our works indicate, that the electrospinning of G and P as a nanofibrous matrix (Nagiah et al., 2013b), collagen coated (Ramanathan et al., 2016) and dual layered (Singaravelu et al., 2017) nanofibrous scaffold act as a promising material for excision type wound healing. Nevertheless, the polymers G and P act as a substrate for cell adhesion, proliferation, complete re-epithelialization and synthesis of collagen in wound healing process. Based on these results, G and P were chosen as a matrix to deliver AgSD adsorbed on LDH to accelerate healing of burn

wounds. Thus, the fabricated GP-(L-AgSD)$_n$ matrix was studied thoroughly for its physicochemical, drug release behavior, biological and mechanical properties as a biomaterial in tissue engineering application. The *in vivo* wound healing ability of the electrospun nanofibrous matrix was assessed by using male Wistar rats to assess the rate of wound closure.

2. Experimental Methods

The experimental methods to synthesis Mg:Al LDH, drug adsorption on LDH and drug loading efficiency on LDH was well explained in the supplementary information.

2. 1. Electrospinning of nanofiber matrices with L-AgSD hybrid

Equal concentrations of G and P were prepared by dissolving them separately in HFIP under constant stirring (4 wt/vol%). To achieve an optimum drug release from the electrospun matrix for effective inhibition against infection at the wound site, various quantities of L-AgSD namely 5, 25 and 50 mg was added to 5 mL of the polymer solution containing G:P in the ratio 30:70 for spinning (Nagiah et al., 2013b). After electrospinning, the electrospun samples were named as GP-(L-AgSD)$_n$ where n is the mass of L-AgSD in milligrams added to 5 mL of the polymer solution. The detailed experimental part was well explained in the supplementary information.

2. 2. Characterization studies of the L-AgSD hybrid and GP-(L-AgSD)$_n$ nanofibrous matrix

All the Characterization methods like X-ray diffraction pattern, Fourier transform infrared (FTIR) spectrum, Thermo gravimetric analysis (TGA), High Resolution Scanning Electron Microscopy (HR-SEM), Atomic Force Microscopy (AFM), and Contact angle was performed in this study was well explained in the supplementary information. The porosity (Jithendra et al., 2013) and swelling index (Taepaiboon et al., 2006) of the nanofibrous matrix was investigated. The detailed experimental part was well explained in the supplementary information. The mechanical property of the all the nanofibrous matrices were analyzed by cutting the nanofibrous

matrices into dumb-bell shaped specimens (100 x 16 mm^2), and the load–elongation measurement was measured using a universal testing machine (INSTRON model 1405) according to Vogel at an extension rate of 5 mm/min (Muthukumar et al., 2014). The rate of degradation of the nanofibrous matrix was determined by using collagenase enzyme (Zhong et al., 2007). The *in vitro* release pattern was studied for all the three formulations using Franz diffusion apparatus (Chakraborti et al., 2012). The antibacterial inhibition test (Xing et al., 2010) and in vitro bacterial viability assay (Arakha et al., 2015) was performed to the nanofibrous matrix. The detailed experimental part was well explained in the supplementary information. The Hemocompatibility assay (Vatankhah et al., 2014) was carried out to determine whether these nanofibrous matrices are hemocompatible with fresh blood when used for *in vivo* application. The MTT assay, cell attachment and proliferation were performed to assess the cell viability of the electrospun nanofibrous matrix using NIH 3T3 fibroblast cell line (Ramanathan et al., 2016). The detailed experimental part was well explained in the supplementary information.

2. 3. In vivo animal studies: Burn wound model

Eighty-four male Albino Wistar rats weighing 190-220 g were individually housed in temperature and humidity-controlled room, monitored continuously with feed and water *ad libitum*. They were randomly divided into seven groups with twelve animals in each group (Non-infected control, infected control, GP-$(L\text{-}AgSD)_{25}$, GP, GP-AgSD, GP-L, standard formulation Silvadene® cream). Three animals were sacrificed from each group at regular intervals. The Institutional Animal Ethics Committee (IAEC) approved the experimental protocols that were performed.

2. 3. 1. Experimental design

A temperature-controlled soldering rod attached with a circular iron disc of 10 mm diameter was used to impose second-degree burn injury on rat models (Shanmugasundaram et al., 2009). The disc was preheated to 82°C-86°C and allowed to stand for 20 minutes to stabilize the temperature. It was then placed over the shaved and disinfected dorsal side of the rats for 20 seconds without applying any external pressure. Before creation of the burn wounds, all the rats were initially anaesthetized using thiopental sodium (22-24 mg/kg body weight).

Fig. 1[a] shows the induction of burn wound in rat. The γ-ray sterilized electrospun matrix was cut into 1.5 cm x 1.5 cm and placed on the surface of the wound using sterile forceps. For the experimental control (group 1 and 2), sterile cotton gauze was placed on the wound site. The wound dressing material was changed periodically at an interval of 4 days (4^{th}, 8^{th}, 12^{th}, 16^{th} day) and three rats in each group were euthanized to collect the granulation tissue.

The induction of microbial infection (Grzybowski et al., 1999), wound healing assessment and estimation of hydroxyproline and hexosamine content in the granulation tissues were determined by the method of Woessner (J. Woessner, 1961), and Elson and Morgan (Elson and Morgan, 1933) respectively. Moreover, the assessment of regulatory cytokines during the *in vivo* studies were performed for the expression of inflammatory cytokines like TNFα, MMP2 and MMP9**.** The detailed experimental part was well explained in the supplementary information.

2. 4. Statistical analysis

All statistical evaluations were carried out using Graph Pad Prism 5 software (Graph Pad Software, San Diego, CA). The results were expressed as mean ± SEM. Statistically significant differences (*P*) were analyzed either by a one or two-way ANOVA with Tukey's post-hoc testing. A value of $P < 0.05$ was statistically significant.

3. Results and discussion

For the easy understanding of the readers, first the characterization results for L-AgSD hybrid material had been discussed, followed by the results for GP-(L-AgSD)$_n$ electrospun nanofibrous matrix.

3. 1. L-AgSD hybrid characterization

3. 1. 1. XRD analysis

The XRD spectra of the composite were given in **Fig. 1[c]** and structure of AgSD was depicted in **Fig. 1[b]**. LDH (Mg:Al) exhibits the pattern of typical crystalline hydrotalcite phase (JCPDS no. 14-0191) which has hexagonal lattice with rhombohedral symmetry and layered features. The main characteristic reflection of L-AgSD hybrid centered at 11.5°, 23.2° and 34.7° can be indexed to (003), (006) and (009) planes of Mg:Al LDH (S. S. L. Sobhana et al., 2016) and the reflections at 8.9°, 10.3° and 18.6° are ascribed to (002), (011) and (020) planes of AgSD which indicates the intrinsic structure of AgSD. The diffraction pattern further reveals that the drug AgSD has occupied the brucite layers by adsorption rather occupying the interlayers of the heterostructure. This was confirmed by the pattern exhibited by L-AgSD where the 003 reflection does not show any shift when compared to the reference LDH and AgSD. Thus, the method for the synthesis was carefully chosen to attain crystallinity for better adsorption of our targeted drug on the cationic layers for further wound healing applications. The pattern also clearly reveals that there was no formation of any secondary phases or impure phases in the form of MgO which might form during the aging process (Klemkaite et al., 2011). Therefore, the co-precipitation method adopted for synthesis has greatly favored the formation of phase pure Mg:Al LDH. Adsorption was more predominant since there was no shift in the diffraction pattern of the final hybrid material compared to LDH alone.

3. 1. 2. FTIR analysis

The adsorption of AgSD on LDH was verified by mid-infrared spectroscopy. **Fig. 1[d]** shows the FTIR spectra of LDH, AgSD, and L-AgSD respectively. The broad absorption band at 3492 cm^{-1} corresponds to the stretching of –OH groups in the brucite-like layer and physiosorbed water.(Pan et al., 2010) For pure AgSD, the band at 1596 cm^{-1} was assigned to vibrational stretching of its phenyl structure conjugated to the NH_2 group (Chakavala et al., 2012; El-feky et al., 2017), the band at 1656 cm^{-1} attributed to NH_2 bending (El-feky et al., 2017) and the band at 1352 cm^{-1} was ascribed to the asymmetrical stretching of the S=O bonding (Chakavala et al., 2012; Li et al., 2015). The structural evaluation of the material before and after treating LDH with AgSD drug reveals that pristine Mg:Al LDH has carbonate groups in the site of intercalation between the layers. The precursors used for the synthesis of this material were nitrate based salts but the FTIR spectrum shows that the intercalated anion was carbonate which clearly shows that carbonate has the highest tendency to enter the galleries of LDH than any other anions. The weak band at 1624 cm^{-1} is due to the water deformation mode. A series of bands recorded in the low wavenumber region can be ascribed to Mg:Al-OH, Al-OH translation modes and Al-OH deformation. All these observations indicate the adsorption of AgSD on LDH.

3. 1. 3. Thermal analysis

The thermogram of LDH (**Fig. 1[e])** shows a gradual mass loss till 224°C which may be attributed to the loss of adsorbed water molecules and those found in the interlayers of the LDH lamellae. The mass loss continues as the temperature increases from 225 to 500°C which corresponds to the loss of hydroxyl groups from the brucite like layer along with the release of interlayer carbonate anions resulting in the formation of mixed metal oxides with disrupted layered structure. The mass loss of this region was also attributed to the loss of water and CO_2

through slow decomposition of the inorganic phases after the disruption of the hydrotalcite. A similar trend has been reported for MgAl LDH intercalated with carbonate anions (Klemkaite et al., 2011) and ZnAl LDH synthesized using cellulose as a biotemplate (S. S. L. Sobhana et al., 2016). In the case of AgSD, the first decomposition occurs from 283 to 329°C which can be attributed to aminopyrimidine decomposition. The second mass loss observed from 420 to 650°C can be assigned to the aromatic ring and sulfur dioxide decomposition and the profile obtained highly correlates with the trend obtained for AgSD containing corn starch and cellulose extrudate matrix (Zepon et al., 2014). From the thermogram, it is evident that there is no significant change in mass loss between free drug and AgSD adsorbed on LDH. However, when the developed scaffold is applied as a burn wound dressing, the drug present in the composite will remain stable at an average body temperature.

3. 1. 4. Particle size distribution and zeta potential

The particle size distribution and zeta potential of LDH and AgSD adsorbed LDH were measured using dynamic light scattering analysis. The hydrodynamic diameter (Z_{av}) of LDH was 258 nm and the calculated polydispersity index (PDI) was 0.212 which was indicative of monodispersed size distribution **(Fig. 1[f])**. On adsorption of AgSD, the resultant L-AgSD nanohybrid powder showed marginal increase in the average particle size (Z_{av}) to 380 nm and PDI of 0.08. The zeta potential of as-synthesized LDH was +30.7 mV denoting a moderately stable suspension which is attributed to the positively charged layers of LDH. A study reported by Fang et al. had discussed the pH-dependent surface charge of MgAl LDH wherein ζ in the range of +30 to +40 mV was obtained for pH 7-8 and it corroborates well with our observation (Fang et al., 2015). The electrokinetic potential of L-AgSD hybrid was obtained to be -45.2 mV which implies an equilibrium binding of drug molecules onto the surface of LDH yielding a

more stable suspension. A stable complex of LDH-MTX was prepared which displayed a zeta potential of +36.3 mV which falls well within the stable range (Chakraborty et al., 2013).

3. 1. 5. Morphology analysis using SEM

Microscopic image of as-synthesized Mg:Al LDH are composed of a large number of typical flat hexagonal plate-like crystals (**Fig. 2[a]**) Similar hexagonal plate-like structures were reported for MgAl LDH by Gu et al. (Gu et al., 2008) and Shafiei et al (Shafiei et al., 2016). The chemical composition of pristine LDH determined by elemental analysis revealed that the ratio of metal ions was 2:1 (**Fig. 2[b]**). The hybrid L-AgSD shows a cloudy appearance of the drug being adsorbed on the surface of LDH. The flaky structure of LDH was not hampered during the formation of L-AgSD hybrids (**Fig. 2[c]**). This type of structure was anticipated in our study for the purpose of drug release from the matrix to the wound site. The L-AgSD hybrid shows the presence of Ag and S peaks arising from AgSD in the hybrid material (**Fig. 2[d]**).

3. 2. Characterization of the electrospun nanofibrous matrix

3. 2. 1. XRD analysis

The X-ray diffraction patterns were analyzed for all matrices to investigate its crystalline structure as reported in **Fig. 2[e]**. The X-ray diffraction pattern of all the nanofibrous matrices show a broad gelatin reflection at 22° and a sharp reflection at approximately 13° attributing to the crystalline nature of poly-(3-hydroxybutyric) acid **(Fig. 2[e](A)).** A control matrix loaded only with AgSD shows the characteristic reflection of AgSD (**Fig. 2[e](B)**). Both the drug and the polymer present higher crystallinity than LDH, which can avoid the visualization of LDH peaks (Fig. 2[e](C-F)). However, this lower structural order of LDH had resulted in its successive dispersion into the nanofibrous matrix. A study on LDH/AMOX incorporated into

PCL nanofibers shows that the nanohybrid has distorted layers of hydroxides upon drug incorporation, thereby enabling its uniform distribution (Valarezo et al., 2013a).

3. 2. 2. Thermal analysis

Thermogravimetric analysis was performed for all the nanofibrous matrices. A three-step mass loss was observed for all samples. The first mass loss observed between 30 and 95°C corresponding to the loss of moisture from gelatin was higher for increasing composition of L-AgSD complex as shown from $T_{-5\%}$ values in **Fig. 2[f]**. Naveen et al. had obtained a similar thermal degradation pattern for Gel-PHB nanofibers (Nagiah et al., 2013b). The second mass loss occurring between 200 and 270°C arises from the dehydroxylation of the layers of LDH. The various amounts of L-AgSD in the nanofibrous matrix did not produce a further relevant decrease in the melting peak (T_m) as shown in **Table S1**. As the temperature approached 800°C, it was observed that 20% of matrix loaded with 25 and 50 mg of L-AgSD still remained as residue whereas the matrix with lowest L-AgSD complex and without the drug was almost thermally decomposed completely. Thus, the incorporation of L-AgSD complex had imparted thermal stability to the polymeric nanofibrous matrix.

3. 2. 3. Morphology analysis using SEM

The surface morphology of the nanofibrous matrices were analyzed using HR-SEM. **Fig. 3[a]** and **Fig. 3[b]** depicts that these nanofibers are randomly oriented and possess a bead-free well interconnected network structure. The L-AgSD particles were seen embedded on the fibers in the concentration studied and was distributed throughout the entire electrospun nanofibrous matrices (Qing Qin, Ya Liu, Si-Chong Chen, Fei-Yu Zhai, Xin-Ke Jing, 2012). The diameter of GP nanofibers ranges from 120-140 nm and those of L-AgSD impregnated electrospun nanofibrous

matrix were also apparently the same. The microscopic images of the nanofibrous matrix also exhibited a porous structure which was later confirmed by a higher swelling index.

3. 2. 4. Atomic force microscopy

Fig. 3([A-D]) shows the 3D topographic surfaces of the electrospun matrices. The surface roughness was determined using Gwyddion AFM data processing software. The microtopographic images reveal rigidity and discrete altitude variations. It was determined to be 29.51 ± 3.25 nm for matrix containing GP and the roughness gradually increased as the ratio of L-AgSD incorporation into the polymer matrix increased. The values were calculated to be 31.24 ± 2.73 nm, 36.06 ± 3.20 nm and 40.03 ± 1.86 nm for matrix having 5, 25 and 50 mg of L-AgSD respectively. Parvinzadeh et al. had reported that the surface roughness of poly ethylene terephthalate based nanocomposites increases by the addition of modified nanoclays (Parvinzadeh et al., 2010). Manikandan et al. had showed that roughness of polyurethane nanocomposite was enhanced by incorporation of murivenna oil favoring hemocompatibility (Manikandan et al., 2017). This result suggests this type of microenvironment to be a suitable surface for cell adhesion.

3. 2. 5. Porosity

The diffusion of gases, metabolite, nutrients and molecular signals between the matrix and the surrounding system makes the nanofibrous matrix more susceptible to mimic the nature of the ECM architecture for cell penetration and proliferation. Thus, porosity plays a critical parameter for nanofibrous matrix. As the concentration of L-AgSD complex increases in the nanofibrous matrix, the porosity seems to gradually decrease (**Fig. 4[a]**). The porosities were 71.5% for GP, 69.4%, 66.8% and 64.3% for matrix with containing 5, 25 and 50 mg of L-AgSD respectively. Moreover, the obtained porosity was more adequate for a wound dressing material to promote

moisture and oxygen exchange. Chandrasekaran et al., has reported with poly(L-lactic acid)-co-poly(ε-caprolactone) nanofibers with a porosity of 84% has been suitable biomaterial in skin regeneration (Chandrasekaran et al., 2011).

3. 2. 6. Contact angle measurement

The surface wettability of a biomaterial will affect cell adhesion, migration, and proliferation of cells (Lin et al., 2012; Liu et al., 2017). For this reason, the water contact angles of all electrospun matrices were determined as shown in **Fig. 4[b]**. As expected, the matrix containing a blend of polymers is more hydrophilic in nature with a contact angle of 60.35°. Moreover, the extent of wettability decreased as the ratio of L-AgSD content increased in the electrospun nanofibrous matrix and it was determined to be 69.62°, 75.31° and 89.62° for 5, 25 and 50 mg respectively. This reduction in hydrophilicity was attributed to the well-known fact that the L-AgSD complex was hydrophobic and hence hinders the extent of wettability. Thus, it was confirmed that the developed matrix has the desired hydrophilicity as a wound dressing material. It is a pre-requisite for any scaffold to be hydrophilic so that it enhances the ability of cells to adhere, proliferate and absorb wound exudates. A study on the composite scaffold using polylactic acid m(PLA) and a biodegradable elastomer, poly (1, 8-octanediol-co-citric acid) also found that the hydrophilic nature of the scaffold was found to be in the range of 99 to 139° (Zou et al., 2019). These studies emphasize the importance of hydrophilicity as a vital factor in the design of a wound dressing material.

3. 2. 7. Swelling index

The determination of the swelling index of the nanofibrous matrix is more important to predict its exudate management and is a vital factor that controls the release of the loaded drug. **Fig. 4[c]** reveals that the swelling percentage of all the matrices lies between 200 and 260% and was

inversely proportional to the L-AgSD complex present in the nanofibrous matrix. It was observed that both the GP containing matrix and that loaded with 5 mg L-AgSD complex reached the swelling saturation after 54 h whereas it was 48 h for higher concentrations of the nanohybrid complex. Xu *et al.* have reported a swelling index of 240% for chitosan/silk microfibers which maintains the necessary conditions for wound healing (Xu et al., 2015). These findings suggest that the fabricated matrix was suitable for tissue engineering application.

3. 2. 8. Mechanical testing

The mechanical properties of the nanofibrous matrices which were designed for direct human application need to be robust enough for both handling and sterilization. **Table 1** exhibited a gradual increase in the tensile strength with increase in the concentration of L-AgSD complexes in the nanofibrous matrix. The mean tensile strength of only the polymeric matrix was 3.12 ± 0.10 MPa and the matrix loaded with 25 mg L-AgSD was 5.32 ± 0.14 MPa. Elongation at break denotes the flexibility of a fabricated material. Increase of L-AgSD had no significant effect on the percentage elongation at break. Mechanical strength analysis of the co-electrospun collagen and zein indicates that the tensile strength of the fabricated material increased with respect to zein concentration (Lin et al., 2012). A similar trend of increase in strength was observed with increasing concentrations of L-AgSD. Shafiei et al. have also reported that the tensile strength of the polymer alone was found to be 1.63 MPa while upon addition of the nanoclay the tensile strength increased to 1.996 MPa (Shafiei et al., 2016). The results obtained and these reports suggest that the nanoclay might influence the stretchability and the tensile strength of the scaffold on a whole.

3. 2. 9. In vitro degradation behavior

The degradation rate and the biological stability of the nanofibrous matrix was evaluated using collagenase enzyme. **Fig. 4[d]** shows that the polymeric nanofibrous matrix exhibited 63.5% mass loss and matrix containing L-AgSD showed 44.8%, 47.9% and 47.6% mass loss with increase in concentration of the drug bound LDH respectively. Accounting to the importance of any biomaterial, biodegradability was an important factor to be considered. An exclusive study on degradation of silk fibroin sheets by several enzymes have been carried out where the degradation rate was determined to be approximately 70% (Li et al., 2003). This signifies the importance of any biomaterial to act as a substrate for proteolytic degradation.

3. 2. 10. In vitro drug release assay

The *in vitro* drug release kinetics of AgSD bound to LDH from the nanofibrous matrices were assessed to investigate the release profile, depending on the controlling parameters *viz.*, drug concentration, fiber diameter and location of the drug with respect to fibers (Valarezo et al., 2013b). The cumulative percentage of AgSD release with respect to time is plotted in **Fig. 4[e]**. After 4 h around 48%, 50% and 56% of AgSD was released from 5, 25 and 50 mg of L-AgSD loaded nanofibrous matrices respectively. This initial burst release of approximately 50% of the drug was desirable and mandatory because any medication intended to control infection at the wound site must exhibit immediate preventive action (chemoprophylaxis) followed by a controlled release up to 72 h. There was a remarkable increase in drug released between 4-12 h after which equilibrium concentration was achieved and maintained till 72 h. In the case of nanofibrous matrix loaded with 50 mg L-AgSD, almost all the drug was released within 72 h. For nanofibrous matrix loaded with 5 and 25 mg L-AgSD, 75% and 86% of the drug had been released over a period of 72 h in a controlled fashion. The nanofibrous matrix with 25 mg L-AgSD released-ptimum measure of drug to combat infection was confirmed by the antimicrobial

studies, which meets the requirements for use as a dressing material. Hence, the scaffold GP-(L-AgSD)$_{25}$ was used for further experiments. Moreover, to prove the need for a carrier molecule to release the drug, the release profile of AgSD from GP-(L-AgSD)$_{25}$ was compared with that of the free drug embedded in the polymeric matrix as illustrated in **Fig. 4[f]**. It was observed that 86% of AgSD had been released in 72 h from the clay nano-hybrid loaded into the matrix compared to the complete release of free drug from the matrix in a short span of time. This difference in release behavior indicates the vital role of LDH as an efficient drug carrier moiety. From these results, it was found that by incorporating AgSD in LDH-polymer film formulations, the antimicrobial activity can be extended over longer durations; a major advantage for a drug eluting wound dressing material.

3. 2. 11. Antibacterial Inhibition and Live/Dead studies

For a wound dressing material to be efficient, the nanofibrous matrix loaded with L-AgSD complex should inhibit the growth of bacterial infection at the wound site. The gradual release of AgSD from the nanofibrous matrix resulted in excellent inhibitory activity against each organism. The scaffold exhibited a MIC and MBC of 48.4 and 52.8 µg/mL against *P. aeruginosa* while *S. aureus* exhibited it as 60.6 and 66.4 µg/mL respectively. Moreover, the viability of the GP-(L-AgSD)$_{25}$ matrix treated against *P. aeruginosa* was further tested using LIVE/DEAD viability assay containing nucleic acid binding dyes. The untreated bacterial cells (**Fig. 4[A]**) were viable and healthy, exhibiting green fluorescence (Arakha et al., 2015). The cells treated with the matrix showed a significant reduction in cell viability as shown in **Fig. 4[B]**. This observation confirms the fact that silver ions from the drug SSD bind to the membrane and disrupt the cellular integrity. This results in the leakage of proteins, disruption of folic acid mechanism, and thereby cell death.

3. 2. 12. In vitro biocompatibility studies

3. 2. 12. 1. Hemolysis assay

Hemocompatiblity was an essential property for a matrix being intended for tissue engineering application. Therefore, any material that induces hemolysis cannot be suitable for wound healing purposes. Our fabricated nanofibrous matrices exhibited no visible signs of hemolysis, compared to the positive control shown in **Fig. 5[a]**. According to standards, samples exhibiting less than 5% are considered to be non-hemolytic (Chen et al., 2008) and the same can be observed in **Fig. 5[b]** which suggests that all electrospun matrices containing varying ratios of L-AgSD were hemocompatible in nature.

3. 2. 12. 2. Co-culturing fibroblasts with electrospun nanofibrous matrix

The biocompatibility of the nanofibrous matrix was determined using MTT assay. The percentage cell viability of the matrices with NIH 3T3 fibroblast cells after 1, 2, 3 and 7 days was exhibited in **Fig. 5[c]**. The cell adhesion and proliferation over the nanofibrous matrix plays aids the construction of the ECM matrix, which will enhance the uniform spreading of cells and healing of wound. The nanofibrous matrix was found to be highly compatible and non-toxic with relative cell viability greater than 90%. Interestingly, with increasing time, more cells proliferated on the matrix which was observed as a significant increase in cell viability. Nonetheless, this proves that these matrices are biocompatible with the presence of LDH and AgSD. *In vitro* fluorescent behavior of the cells over the nanofibrous matrix is depicted in **Fig. 5[d]**. The nanofibrous matrix forms the backbone for the cell adhesion and proliferation. The nanofibrous matrix with 25 mg L-AgSD demonstrated adequate cell adhesion that initiates effective wound healing (Singaravelu et al., 2016). The scaffolds made with PCL-LDH were found to have more viable cells growing on the fibrous matrix (Shafiei et al., 2016). The surface

topography enabled higher percentage of cell adhesion and proliferation. Several studies also suggest that the hybrid with nanoclay had a positive impact on the cell behavior, colonization and the proliferation of the cells (Akhilesh K. Gaharwar et al., 2014). The electrospun gelatin and PHB was found to support dermal keratinocytes and fibroblasts as reported by Nagiah et al. (Nagiah et al., 2013a). All these studies show that the matrix shows good biocompatibility as observed in our study.

3. 2. 13. Progression of wound healing by the nanofibrous matrix

The *in vivo* wound healing efficacy of the nanofibrous matrix was determined by placing the material on the burn wounds. The matrices when placed on the wound site, adhered effortlessly owing to the hydrophilic nature of the polymers which provided adequate moisture and flexibility for application. No mortality was observed throughout the course of experiment. Over the course of wound healing the granulation tissue was collected, and the body weight of the animals was recorded. Influence of the matrix on wound closure at different time points as confirmed by macroscopic analysis is depicted in **Fig. 6**. Similar observations like the rate of wound contraction, biochemical analysis and histological examinations were performed to evaluate the wound healing activity by Mazlyzam et al (AL et al., 2015).

The quantitative wound closure rate was determined by tracing the perimeter of the wound onto a graph sheet at specified time intervals as represented in **Fig. 7[a]**. The group treated with Silvadene® achieved higher wound closure rate of 98 ± 5.8% on day 20. The wound closure rate for the other groups as observed on the twentieth day post-wounding was found to be in the following order: GP-(L-AgSD)$_{25}$ (95 ± 7.3%), GP-AgSD (93 ± 8.2%), GP (88 ± 5.9%), Non-infected control (81 ± 6.8%), GP-L (71 ± 6.2%), infected control (63 ± 4.6%).

3. 2. 14. Body weight assessment

The average body weight of the rats was 207 g. All the control and experimental rats were monitored throughout the study period and body weight was measured and expressed as mean ± standard error (**Fig. 7[b]**). For the animals treated with Silvadene®, there was an initial decrease in the body weight after inducing wound. As the healing of wound progressed, the animals regained their weight. The control and treated groups showed a reduction in body weight on the 4^{th} day post wounding but showed no significant difference from day 16 as the wound healed.

3. 2. 15. Mechanical properties of the granulation tissue

To evaluate the mechanical strength of the newly formed granulation tissue, the tensile strength and % elongation at break was measured. The tissues collected from the euthanized rats at day 20 were cut into lengthwise strips of 3 cm width such that the induced wound area lies at the centre. The tensile strength and elongation at break of all the control and experimental groups were shown in **Fig. 7[c]** and **Fig. 7[d]** respectively. The tensile strength was found to be higher corresponding to the rate of proliferation of cells. The higher tensile strength can be corroborated to the faster rate of wound healing in the groups 3, 5 and 7 which might be due to collagen deposition and re-epithelialization (Choi et al., 2018).

3. 2. 16. Histological examination

The granulation tissue samples were stored in buffered formalin and then stained with haematoxylin and eosin (H&E) as well as Masson's trichome (MT) staining. Paraffin sections of the samples were prepared and examined using light microscopy to evaluate the level of granulation tissue formation and wound re-epithelialization. The burn had resulted in the loss of follicles that are deep in the dermal section. According to the histological figures (**Fig. 8**), the sections of group 3 treated with GP-(L-AgSD) showed minimal necrosis compared to the control

groups. Granulation was initiated after the formation of crest on day 2 in all the groups. The rate of re-epithelialization was similar in groups 3 and 7 when compared to the groups 1 and 2 which showed a lower rate of epithelialization. The sections from the control group show the presence of neutrophils and macrophages indicating an inflammatory response. The infiltration of white cells was found to be decreasing in the Silvadene® treated group. On day 12, neoepidermis formation was observed in group 3 and 7, whereas the control groups had a large open wound area. Towards day 16 a normal pattern of hair growth was observed in the area surrounding the wound site with a thicker epidermis and a good extent of collagen deposition. Restrained healing and a thin epidermal layer are observed in the control group due to microbial load. These results suggest that the controlled release of the drug in the group treated with the complete matrix has successfully controlled the infection and accelerated wound healing.

Masson's trichrome staining was used to study the collagen deposition at the wound site. The deposition of collagen is proportional to the strength and the healing of the wound. On day 12 of group 3 and 7, a pronounced deposition of collagen is observed with densely packed fibers. Well-oriented collagen was seen to be deposited with a thicker granulation tissue in the GP-(L-AgSD)$_{25}$ and Silvadene® treated groups. Uniform distribution of collagen is observed in corroboration with the decreased level of hexosamine as discussed below.

3. 2. 17. Biochemical analysis

The estimation of hydroxyproline was vital in understanding the collagen turnover post-wounding. Collagen was an integral part of the extracellular protein that was present in the granulation tissue. An increase in the level of hydroxyproline indicates an accelerated wound healing as shown in **Fig. 7[e]**. Both the treated and control groups showed a lower hydroxyproline level at day 4 post-wounding. It was also observed that the amino acid content

was at its peak at day 8 which later reduced as the wound healing progressed for Silvadene® treated groups. For group 3, the level was higher at day 12 which aids in rapid healing. On the contrary, the control groups showed an increased collagen content at day 16 which attributes to delayed healing in control groups. Hexosamine molecules form the ground substrate for extracellular matrix. The concentration of hexosamine was seen to be inversely proportional with progression of healing (Udhayakumar et al., 2017). A similar pattern of healing is reported by Mazlyzam et al. where the level of hexosamine was high on day 3 and decreased on day 6 when treated with the stem juice of *A. denudata* (AL et al., 2015). The presence of these glycosaminoglycans aid in stabilization of collagen fibers and facilitate cell adhesion and proliferation. The concentration of hexosamine on 4, 8, 12, and 16th day were monitored which is shown in **Fig. 7[f]**. However, the level of hexosamine was found to diminish gradually with the progress of wound healing and collagen deposition.

3. 2. 18. Assessment of regulatory cytokines

Fig. 9 indicates the immunohistochemical staining of MMP-2, MMP-9, TNFα post-burn wound days. The regulation of growth factors and the proteinase activity by MMP's play a dynamic role in the reconstruction of wound. So, in this study the expression of MMP during the course of healing was assessed (Shanmugasundaram et al., 2009). The level of MMP 2 and 9 was seen to be high in the samples taken on day 4 in all the groups. However, as the days progressed the expression of MMPs'diminished. In the non-infected group, MMP levels was reduced in day 8 while the infected groups showed higher levels of MMP because of the infection which hindered healing. A gradual decrease in the MMP expression was observed with the advancement of wound healing. The level of MMP 2 diminished from day 12 to undetectable levels from day 16 onwards which was also confirmed through gelatin zymography. As observed in the

immunohistochemical staining, the expression of MMP 2 seen in groups treated with Silvadene® and the nanoconstruct, induced cellular migration and thereby initiation of cell adhesion. The MMP-9 expressed in the same groups on day 8 aids in the re-epithelialization at the edges of the wound which is evidenced by the histochemical studies. Shanmugasundaram et al. had reported that the levels of MMP 2 was seen to be higher in the intial days after wounding while the expression of MMP 9 was profound as wound healing progressed. (Shanmugasundaram et al., 2009)

The immunohistochemical studies reveal the presence of the inflammatory cytokine (tumor necrosis factor α) indicating the preparatory process of wound healing. TNFα being an important inflammatory marker stimulates the adhesion and differentiation of fibroblasts. Its expression was observed in day 4 of group 3 and gradually reduced as wound healing progressed. Zhu et al. had reported that the expression of TNFα decreased in SA/GMs/Dex-HA hydrogel applied to full-thickness infected burn wound rat models (Zhu et al., 2018). When re-epithelialization begins, MMP's were observed which play a major role in degrading the ECM allowing vascularisation to begin. Thus, the presence of these cytokines signifies the induction of inflammation leading to angiogenesis upon treatment with the scaffold. **Fig. 9** indicates the immunohistochemical staining of MMP-2, MMP-9, TNFα in the burn wound treated with the scaffold (group 3)

4. Conclusion

In summary, the prospect of this study was designed perceiving the aspects of a burn patient with wound infection. Electrospinning of Poly-3-hydroxybutyric acid (P) and gelatin (G) yielded a nanofibrous matrix with excellent porosity, swelling index, offering the required degradability and mechanical strength. The highly porous morphology enabled oxygen transfer with conducive

environment for adhesion and proliferation of fibroblasts. The mechanical durability of the dressing reduces the strain of frequent dressing and hastens healing. The drug bound LDH, L-AgSD incorporated in the scaffold shielded the wound from infection at the tested concentration. *In-vivo* wound healing efficiency of the burn wounds were promising with the use of L-AgSD augmented nanofibrous construct. overall, the nanofibrous construct exhibited a positive influence on the process of wound healing in all perspectives.

Acknowledgement

The author Vimala Devi Mohan gratefully acknowledges financial support for this work through the grants awarded by the Department of Science and Technology (DST), New Delhi, India, (SR/WOS-A/ET-1060/2014). Financial support from ICMR (IRIS No.2013-1293.) and CSIR-CLRI under Translational Research Project OLP-09/TRP is acknowledged.

Author contributions

The manuscript was written through contributions of all authors. All authors have given approval to the final version of the manuscript.

Notes

The authors declare no competing financial interest.

Supplementary Information

Table S1 and detailed experimental methods section is given as supplementary information

References

Akhilesh K. Gaharwar, S.M., Karaca, E., Dolatshahi-Pirouz, A., Patel, A., Rangarajan, K., Silvia M. Mihaila, Iviglia, G., Zhang, H., Ali, K., 2014. Nanoclay-enriched poly(ε-caprolactone) electrospun scaffolds for osteogenic differentiation of human mesenchymal stem cells. TISSUE Eng. Part A 20, 2088–2101.

AL, M., Zaki, M.Z.M., Leng, T.M., Rahman, N.H.A., Arshad, S.A., Hamid, A., 2015. Alocasia denudata Engler treatment enhance open wound healing activities in Wistar rat's skin. J. Ethnopharmacol. 176, 258–267. https://doi.org/10.1016/j.jep.2015.10.036

Andreu, V., Mendoza, G., Arruebo, M., Irusta, S., 2015. Smart dressings based on nanostructured fibers containing natural origin antimicrobial, anti-inflammatory, and regenerative compounds. Materials (Basel). 8, 5154–5193. https://doi.org/10.3390/ma8085154

Arakha, M., Pal, S., Samantarrai, D., Panigrahi, T.K., Mallick, B.C., Pramanik, K., Mallick, B., Jha, S., 2015. Antimicrobial activity of iron oxide nanoparticle upon modulation of nanoparticle-bacteria interface. Sci. Rep. 5, 1–12. https://doi.org/10.1038/srep14813

Budyanto, L., Goh, Y.Q., Ooi, C.P., 2009. Fabrication of porous poly(L-lactide) (PLLA) scaffolds for tissue engineering using liquid-liquid phase separation and freeze extraction. J. Mater. Sci. Mater. Med. 20, 105–111. https://doi.org/10.1007/s10856-008-3545-8

Chakavala, S.R., Patel, N.G., Thakkar, V.T., Patel, K. V, Gandhi, T.R., 2012. Development and in vivo evaluation of silver sulfadiazine loaded hydrogel consisting polyvinyl alcohol and chitosan for severe burns. J Pharm Bioall Sci 4, 54–57. https://doi.org/10.4103/0975-7406.94131

Chakraborti, M., Jackson, J.K., Plackett, D., Gilchrist, S.E., Burt, H.M., 2012. The application of layered double hydroxide clay (LDH)-poly(lactide-co- glycolic acid) (PLGA) film composites for the controlled release of antibiotics. J. Mater. Sci. Mater. Med. 23, 1705–1713. https://doi.org/10.1007/s10856-012-4638-y

Chakraborty, J., Roychowdhury, S., Sengupta, S., Ghosh, S., 2013. Mg-Al layered double hydroxide-methotrexate nanohybrid drug delivery system: Evaluation of efficacy. Mater.

Sci. Eng. C 33, 2168–2174. https://doi.org/10.1016/j.msec.2013.01.047

Chandrasekaran, A.R., Venugopal, J., Sundarrajan, S., Ramakrishna, S., 2011. Fabrication of a nanofibrous scaffold with improved bioactivity for culture of human dermal fibroblasts for skin regeneration. Biomed. Mater. 6. https://doi.org/10.1088/1748-6041/6/1/015001

Chen, C., Cheng, Y.C., Yu, C.H., Chan, S.W., Cheung, M.K., Yu, P.H.F., 2008. In vitro cytotoxicity, hemolysis assay, and biodegradation behavior of biodegradable poly(3-hydroxybutyrate)-poly(ethylene glycol)-poly(3- hydroxybutyrate) nanoparticles as potential drug carriers. J. Biomed. Mater. Res. - Part A 87, 290–298. https://doi.org/10.1002/jbm.a.31719

Choi, H.M.C., Cheing, A.K.K., Ng, G.Y.F., Cheing, G.L.Y., 2018. Effects of pulsed electromagnetic field (PEMF) on the tensile biomechanical properties of diabetic wounds at different phases of healing 1–12.

Dai, M., Zheng, X., Xu, X., Kong, X., Li, X., Guo, G., Luo, F., Zhao, X., Wei, Y.Q., Qian, Z., 2009. Chitosan-Alginate Sponge : Preparation and Application in Curcumin Delivery for Dermal Wound Healing in Rat 2009. https://doi.org/10.1155/2009/595126

El-Feky, G.S., El-Banna, S.T., El-Bahy, G.S., Abdelrazek, E.M., Kamal, Em., 2017. Alginate coated chitosan nanogel for the controlled topical delivery of Silver sulfadiazine. Carbohydr. Polym. 177, 194–202. https://doi.org/10.1016/j.carbpol.2017.08.104

Elson, L.A., Morgan, and W.T.J., 1933. A COLORIMETRIC METHOD FOR THE DETERMINATION OF GLUCOSAMINE AND CHONDROSAMINE.

Fallah, M., Bahrami, S.H., Ranjbar-Mohammadi, M., 2016. Fabrication and characterization of PCL/gelatin/curcumin nanofibers and their antibacterial properties. J. Ind. Text. 46, 562–577. https://doi.org/10.1177/1528083715594978

596 Fang, L., Li, W., Chen, H., Xiao, F., Holm, P.E., Hansen, C.B., 2015. Synergistic effect of humic
597 and fulvic acids on Ni removal by the calcined Mg / Al 1–7.
598 Garg, T., Singh, O., Arora, S., Murthy, R.S.R., 2012. Scaffold: A Novel Carrier for Cell and
599 Drug Delivery. Crit. Rev. Ther. Drug Carr. Syst. 29, 1–63.
600 https://doi.org/10.1615/CritRevTherDrugCarrierSyst.v29.i1.10
601 Ge, N., Wang, D., Peng, F., Li, J., Qiao, Y., Liu, X., 2016. Poly(styrenesulfonate)-Modified Ni-
602 Ti Layered Double Hydroxide Film: A Smart Drug-Eluting Platform. ACS Appl. Mater.
603 Interfaces 8, 24491–24501. https://doi.org/10.1021/acsami.6b09697
604 Grzybowski, J., Janiak, M.K., Oidak, E., Lasocki, K., Wrembel-Wargocka, J., Cheda, A., Antos-
605 Bielska, M., Pojda, Z., 1999. New cytokine dressings. II. Stimulation of oxidative burst in
606 leucocytes in vitro and reduction of viable bacteria within an infected wound. Int. J. Pharm.
607 184, 179–187. https://doi.org/10.1016/S0378-5173(99)00064-2
608 Gu, Z., Thomas, A.C., Xu, Z.P., Campbell, J.H., Lu, G.Q., 2008. In vitro sustained release of
609 LMWH from MgAl-layered double hydroxide nanohybrids. Chem. Mater. 20, 3715–3722.
610 https://doi.org/10.1021/cm703602t
611 Heo, D.N., Yang, D.H., Lee, J.B., Bae, M.S., Kim, J.H., Moon, S.H., Chun, H.J., Kim, C.H.,
612 Lim, H.N., Kwon, I.K., 2013. Burn-wound healing effect of gelatin/polyurethane nanofiber
613 scaffold containing silver-sulfadiazine. J. Biomed. Nanotechnol. 9, 511–515.
614 https://doi.org/10.1166/jbn.2013.1509
615 J. Woessner, J., 1961. The Determination of Hydroxyproline in Tisuue and Protein Samples
616 Containing Small Proportions of this Imino Acid. Arch. Biochem. Biophys. 93, 440–447.
617 Jahromi, M.A.M., Zangabad, P.S., Basri, S.M.M., Zangabad, K.S., Ghamarypour, A., Aref, A.R.,
618 Karimi, M., Hamblin, M.R., 2018. Nanomedicine and advanced technologies for burns:

Preventing infection and facilitating wound healing. Adv. Drug Deliv. Rev. 123, 33–64. https://doi.org/10.1016/j.addr.2017.08.001

Jiang, J., Carlson, M.A., Teusink, M.J., Wang, H., MacEwan, M.R., Xie, J., 2015. Expanding Two-Dimensional Electrospun Nanofiber Membranes in the Third Dimension by a Modified Gas-Foaming Technique. ACS Biomater. Sci. Eng. 1, 991–1001. https://doi.org/10.1021/acsbiomaterials.5b00238

Jin, L., Liu, Q., Sun, Z., Ni, X., Wei, M., 2010. Preparation of 5-fluorouracil/β-cyclodextrin complex intercalated in layered double hydroxide and the controlled drug release properties. Ind. Eng. Chem. Res. 49, 11176–11181. https://doi.org/10.1021/ie100990z

Jithendra, P., Rajam, A.M., Kalaivani, T., Mandal, A.B., Rose, C., 2013. Preparation and characterization of aloe vera blended Collagen-Chitosan composite scaffold for tissue engineering applications. ACS Appl. Mater. Interfaces 5, 7291–7298. https://doi.org/10.1021/am401637c

Kim, S.E., Wang, J., Jordan, A.M., Korley, L.T.J., Baer, E., Pokorski, J.K., 2014. Surface modification of melt extruded poly(μ-caprolactone) nanofibers: Toward a new scalable biomaterial scaffold. ACS Macro Lett. 3, 585–589. https://doi.org/10.1021/mz500112d

Klemkaite, K., Prosycevas, I., Taraskevicius, R., Khinsky, A., Kareiva, A., 2011. Synthesis and characterization of layered double hydroxides with different cations (Mg, Co, Ni, Al), decomposition and reformation of mixed metal oxides to layered structures. Cent. Eur. J. Chem. 9, 275–282. https://doi.org/10.2478/s11532-011-0007-9

Li, M., Ogiso, M., Minoura, N., 2003. Enzymatic degradation behavior of porous silk fibroin sheets. Biomaterials 24, 357–365. https://doi.org/10.1016/S0142-9612(02)00326-5

Li, P., Xu, X., Wu, L., Li, B., Zhao, Y., 2015. Synthesis of silver nanoparticles loaded

642 sulfadiazine/polyvinyl alcohol nanorods and their antibacterial activities. Med. Chem.
643 Commun. 6, 2204–2208. https://doi.org/10.1039/C5MD00331H
644 Liji, L.S., Mehedi, R., Malmivirta, M., Paturi, P., Lastusaari, M., Dîrtu, M.M., Garcia, Y.,
645 Fardim, P., 2016. Heteronuclear nanoparticles supported hydrotalcites containing Ni(II) and
646 Fe(III) stable photocatalysts for Orange II degradation. Appl. Clay Sci. 132–133, 641–649.
647 https://doi.org/10.1016/j.clay.2016.08.016
648 Lin, J., Li, C., Zhao, Y., Hu, J., Zhang, L.M., 2012. Co-electrospun nanofibrous membranes of
649 collagen and zein for wound healing. ACS Appl. Mater. Interfaces 4, 1050–1057.
650 https://doi.org/10.1021/am201669z
651 Liu, J., Lu, F., Chen, H., Bao, R., Li, Z., Lu, B., Yu, K., Dai, F., Wu, D., Lan, G., 2017. Healing
652 of skin wounds using a new cocoon scaffold loaded with platelet-rich or platelet-poor
653 plasma. RSC Adv. 7, 6474–6485. https://doi.org/10.1039/C6RA27021B
654 Manikandan, A., Mani, M.P., Jaganathan, S.K., Rajasekar, R., Jagannath, M., 2017. Formation of
655 functional nanofibrous electrospun polyurethane and murivenna oil with improved
656 haemocompatibility for wound healing. Polym. Test. 61, 106–113.
657 https://doi.org/10.1016/j.polymertesting.2017.05.008
658 Martin, C., Low, W.L., Amin, M.C.I.M., Radecka, I., Raj, P., Kenward, K., 2013. Current trends
659 in the development of wound dressings, biomaterials and devices. Pharm. Pat. Anal. 2, 341–
660 359. https://doi.org/10.4155/ppa.13.18
661 Martín, J., Maiz, J., Sacristan, J., Mijangos, C., 2012. Tailored polymer-based nanorods and
662 nanotubes by "template synthesis": From preparation to applications. Polymer (Guildf). 53,
663 1149–1166. https://doi.org/10.1016/j.polymer.2012.01.028
664 Muthukumar, T., Prabu, P., Ghosh, K., Sastry, T.P., 2014. Fish scale collagen sponge

665 incorporated with Macrotyloma uniflorum plant extract as a possible wound/burn dressing
666 material. Colloids Surfaces B Biointerfaces 113, 207–212.
667 https://doi.org/10.1016/j.colsurfb.2013.09.019
668 Nagiah, N., Madhavi, L., Anitha, R., Anandan, C., Srinivasan, N.T., Sivagnanam, U.T., 2013a.
669 Development and characterization of coaxially electrospun gelatin coated poly (3-
670 hydroxybutyric acid) thin films as potential scaffolds for skin regeneration. Mater. Sci. Eng.
671 C 33, 4444–4452. https://doi.org/10.1016/j.msec.2013.06.042
672 Nagiah, N., Madhavi, L., Anitha, R., Srinivasan, N.T., Sivagnanam, U.T., 2013b.
673 Electrospinning of poly (3-hydroxybutyric acid) and gelatin blended thin films: Fabrication,
674 characterization, and application in skin regeneration. Polym. Bull. 70, 2337–2358.
675 https://doi.org/10.1007/s00289-013-0956-6
676 O'Brien, F.J., 2011. Biomaterials & scaffolds for tissue engineering. Mater. Today 14, 88–95.
677 https://doi.org/10.1016/S1369-7021(11)70058-X
678 Ouyang, Q., Hu, Z., Lin, Z., Quan, W., Deng, Y., Li, S., Li, P., Chen, Y., 2018. International
679 Journal of Biological Macromolecules Chitosan hydrogel in combination with marine
680 peptides from tilapia for burns healing. Int. J. Biol. Macromol. 112, 1191–1198.
681 https://doi.org/10.1016/j.ijbiomac.2018.01.217
682 Pan, D., Zhang, H., Zhang, T., Duan, X., 2010. A novel organic-inorganic microhybrids
683 containing anticancer agent doxifluridine and layered double hydroxides: Structure and
684 controlled release properties. Chem. Eng. Sci. 65, 3762–3771.
685 https://doi.org/10.1016/j.ces.2010.03.013
686 Parvinzadeh, M., Moradian, S., Rashidi, A., Yazdanshenas, M.E., 2010. Effect of the addition of
687 modified nanoclays on the surface properties of the resultant polyethylene terephthalate/clay

nanocomposites. Polym. - Plast. Technol. Eng. 49, 874–884. https://doi.org/10.1080/03602551003664628

Qing Qin, Ya Liu, Si-Chong Chen, Fei-Yu Zhai, Xin-Ke Jing, Y.Z.W., 2012. Electrospinning Fabrication and Characterization of Poly(vinyl alcohol)/Layered Double Hydroxides Composite Fibers. J. Polym. Appl. Sci. 126. https://doi.org/10.1002/app.36876

Qiu, D. peng, Hou, W. guo, 2009. Synthesis and characterization of indole-3-butyric acid/hydrotalcite-like compound nanohybrids. Colloids Surfaces A Physicochem. Eng. Asp. 336, 12–17. https://doi.org/10.1016/j.colsurfa.2008.11.028

Ramanathan, G., Singaravelu, S., Raja, M.D., Nagiah, N., Padmapriya, P., Ruban, K., Kaveri, K., Natarajan, T.S., Sivagnanam, U.T., Perumal, P.T., 2016. Fabrication and characterization of a collagen coated electrospun poly(3-hydroxybutyric acid)-gelatin nanofibrous scaffold as a soft bio-mimetic material for skin tissue engineering applications. RSC Adv. 6, 7914–7922. https://doi.org/10.1039/c5ra19529b

Rathore, H.S., Sarubala, M., Ramanathan, G., Singaravelu, S., Raja, M.D., Gupta, S., Sivagnanam, U.T., 2016. Fabrication of biomimetic porous novel sponge from gum kondagogu for wound dressing. Mater. Lett. 177, 108–111. https://doi.org/10.1016/j.matlet.2016.04.185

Sano, S., Fujimori, R., Takashima, M., Itokawa, Y., 1982. Absorption, excretion and tissue distribution of silver sulfadiazine. Burns 8, 278–285. https://doi.org/10.1016/0305-4179(82)90010-9

Shafiei, S.S., Shavandi, M., Ahangari, G., Shokrolahi, F., 2016. Electrospun layered double hydroxide/poly (ε-caprolactone) nanocomposite scaffolds for adipogenic differentiation of adipose-derived mesenchymal stem cells. Appl. Clay Sci. 127–128, 52–63.

711 https://doi.org/10.1016/j.clay.2016.04.004
712 Shafiei, S.S., Solati-Hashjin, M., Samadikuchaksaraei, A., Kalantarinejad, R., Asadi-Eydivand,
713 M., Abu Osman, N.A., 2015. Epigallocatechin gallate/layered double hydroxide
714 nanohybrids: Preparation, characterization, and in vitro anti-tumor study. PLoS One 10, 1–
715 18. https://doi.org/10.1371/journal.pone.0136530
716 Shanmugasundaram, N., Uma, T.S., Lakshmi, T.S.R., Babu, M., 2009. Efficiency of controlled
717 topical delivery of silver sulfadiazine in infected burn wounds. J. Biomed. Mater. Res. - Part
718 A 89, 472–482. https://doi.org/10.1002/jbm.a.31997
719 Shao, W., Wu, J., Wang, S., Huang, M., Liu, X., Zhang, R., 2017. Construction of silver
720 sulfadiazine loaded chitosan composite sponges as potential wound dressings. Carbohydr.
721 Polym. 157, 1963–1970. https://doi.org/10.1016/j.carbpol.2016.11.087
722 Singaravelu, S., Ramanathan, G., Sivagnanam, U.T., 2017. Dual-layered 3D nanofibrous matrix
723 incorporated with dual drugs and their synergetic effect on accelerating wound healing
724 through growth factor regulation. Mater. Sci. Eng. C 76, 37–49.
725 https://doi.org/10.1016/j.msec.2017.02.148
726 Smith, L.A., Ma, P.X., 2004. Nano-fibrous scaffolds for tissue engineering. Colloids Surfaces B
727 Biointerfaces 39, 125–131. https://doi.org/10.1016/j.colsurfb.2003.12.004
728 Sobhana, L., Sarakha, M., Prevot, V., Fardim, P., 2016. Layered double hydroxides decorated
729 with Au-Pd nanoparticles to photodegradate Orange II from water. Appl. Clay Sci. 134,
730 120–127. https://doi.org/10.1016/j.clay.2016.06.019
731 Sobhana, S.S.L., Bogati, D.R., Reza, M., Gustafsson, J., Fardim, P., 2016. Cellulose
732 biotemplates for layered double hydroxides networks. Microporous Mesoporous Mater.
733 225, 66–73. https://doi.org/10.1016/j.micromeso.2015.12.009

734 Sobhana, S.S.L., Zhang, X., Kesavan, L., Liias, P., Fardim, P., 2017. Layered double hydroxide
735 interfaced stearic acid – Cellulose fibres: A new class of super-hydrophobic hybrid
736 materials. Colloids Surfaces A Physicochem. Eng. Asp. 522, 416–424.
737 https://doi.org/10.1016/j.colsurfa.2017.03.025
738 Taepaiboon, P., Rungsardthong, U., Supaphol, P., 2006. Drug-loaded electrospun mats of
739 poly(vinyl alcohol) fibres and their release characteristics of four model drugs.
740 Nanotechnology 17, 2317–2329. https://doi.org/10.1088/0957-4484/17/9/041
741 Timmers, M.S., Graafland, N., Bernards, A.T., Nelissen, R.G.H.H., Dissel, J.T. Van, Jukema,
742 G.N., 2008. Negative pressure wound treatment with polyvinyl alcohol foam and
743 polyhexanide antiseptic solution instillation in posttraumatic osteomyelitis.
744 https://doi.org/10.1111/j.1524-475X.2009.00458.x
745 Udhayakumar, S., Shankar, K.G., Sowndarya, S., 2017. RSC Advances engineering and
746 regeneration : in silico , in vitro , and. RSC Adv. 7, 25070–25088.
747 https://doi.org/10.1039/C7RA02842C
748 Unnithan, A.R., Barakat, N.A.M., Tirupathi Pichiah, P.B., Gnanasekaran, G., Nirmala, R., Cha,
749 Y.S., Jung, C.H., El-Newehy, M., Kim, H.Y., 2012. Wound-dressing materials with
750 antibacterial activity from electrospun polyurethane-dextran nanofiber mats containing
751 ciprofloxacin HCl. Carbohydr. Polym. 90, 1786–1793.
752 https://doi.org/10.1016/j.carbpol.2012.07.071
753 Valarezo, E., Tammaro, L., González, S., Malagón, O., Vittoria, V., 2013b. Fabrication and
754 sustained release properties of poly(ε-caprolactone) electrospun fibers loaded with layered
755 double hydroxide nanoparticles intercalated with amoxicillin. Appl. Clay Sci. 72, 104–109.
756 https://doi.org/10.1016/j.clay.2012.12.006

Vatankhah, E., Prabhakaran, M.P., Semnani, D., Razavi, S., Morshed, M., Ramakrishna, S., 2014. Electrospun tecophilic/gelatin nanofibers with potential for small diameter blood vessel tissue engineering. Biopolymers 101, 1165–1180. https://doi.org/10.1002/bip.22524

Williams, G.R., Dunbar, T.G., Beer, A.J., Fogg, A.M., O'Hare, D., 2006. Intercalation chemistry of the novel layered double hydroxides MAl4(OH)(12) (NO3)(2)center dot gamma H2O (M = Zn, Cu, Ni and Co). 1: New organic intercalates and reaction mechanisms. J. Mater. Chem. 16, 1222–1230. https://doi.org/10.1039/b514874j

Xing, Z.C., Chae, W.P., Baek, J.Y., Choi, M.J., Jung, Y., Kang, I.K., 2010. In vitro assessment of antibacterial activity and cytocompatibility of silver-containing phbv nanofibrous scaffolds for tissue engineering. Biomacromolecules 11, 1248–1253. https://doi.org/10.1021/bm1000372

Xu, Z., Shi, L., Yang, M., Zhang, H., Zhu, L., 2015. Fabrication of a novel blended membrane with chitosan and silk microfibers for wound healing: characterization, in vitro and in vivo studies. J. Mater. Chem. B 3, 3634–3642. https://doi.org/10.1039/C5TB00226E

Zepon, K.M., Petronilho, F., Soldi, V., Salmoria, G.V., Kanis, L.A., 2014. Production and characterization of cornstarch/cellulose acetate/silver sulfadiazine extrudate matrices. Mater. Sci. Eng. C 44, 225–233. https://doi.org/10.1016/j.msec.2014.08.011

Zhong, S.P., Teo, W.E., Zhu, X., Beuerman, R., Ramakrishna, S., Yung, L.Y.L., 2007. Development of a novel collagen-GAG nanofibrous scaffold via electrospinning. Mater. Sci. Eng. C 27, 262–266. https://doi.org/10.1016/j.msec.2006.05.010

Zhu, Q., A, Jiang, M., A, Liu, Q., B, Yan, S., A, Feng, L., A, Lan, Y., C, Shan, G., D, Xue, W.G., 2018. Enhanced Healing Activity of Burn Wound Infection by Dextran-HA Hydrogel Enriched with Sanguinarine. Biomater. Sci. 6, 2472–2486.

https://doi.org/10.1039/C8BM00478A

Zou, F., Sun, X., Wang, X., 2019. Elastic, hydrophilic and biodegradable poly (1, 8-octanediol-co-citric acid)/polylactic acid nanofibrous membranes for potential wound dressing applications. Polym. Degrad. Stab. 166, 163–173.

Table captions

Table 1 Mechanical properties of electrospun nanofibrous matrices

Figure Captions

Figure 1 [a] Creation of burn wound with a temperature-controlled soldering rod, [b] Structure of silver sulfadazine (AgSD), [c] X-ray diffractogram of as-synthesized LDH, AgSD and L-AgSD. * denotes AgSD reflections and # denotes LDH reflections, [d] FTIR spectrum of as-synthesized LDH, AgSD and L-AgSD. * denotes AgSD reflections and # denotes LDH reflections, [e] TGA profiles of as-synthesized LDH and L-AgSD, [f] Particle size distribution of as-synthesized LDH and L-AgSD

Figure 2 [a & b] SEM, [c & d] elemental mapping images of MgAl LDH and L-AgSD respectively, [e] X-ray diffractogram of nanofibrous matrix containing (A) GP, (B) GP-AgSD, (C) GP-L, (D) GP-$(L\text{-}AgSD)_5$, (E) GP-$(L\text{-}AgSD)_{25}$ and (F) GP-$(L\text{-}AgSD)_{50}$ and [d] Thermo gravimetric curves of nanofibrous matrix

Figure 3 [a & b] HRSEM micrographs and [c & d] elemental mapping images of GP and GP-$(L\text{-}AgSD)_{25}$ nanofibrous matrix respectively. Inset shows the digital photograph of GP-$(L\text{-}AgSD)_{25}$, Atomic force micrograph of nanofibrous matrix containing [A] GP, [B] GP-$(L\text{-}AgSD)_5$, [C] GP-$(L\text{-}AgSD)_{25}$ and [D] GP-$(L\text{-}AgSD)_{50}$

Figure 4 [a] Porosity measurements of the nanofibrous matrix, [b] Water contact angle of various electrospun nanofibrous matrix, [c] Swelling behavior of the nanofibrous matrix, [d] *In*

vitro degradation of the nanofibrous matrix using collagenase enzyme, [e] *In vitro* drug release profiles of AgSD from electrospun nanofibrous matrix, [f] *In vitro* release profile of AgSD from matrix containing GP-$AgSD_{25}$ and GP-$(L\text{-}AgSD)_{25,}$ Fluorescence microscopy images of *Pseudomonas aeruginosa* (A) untreated and (B) treated with GP-$(L\text{-}AgSD)_{25}$ followed by staining with SYTO 9 and PI. The images were recorded at 40× magnification using a fluorescence microscope

Figure 5 [a] Digital photographs of red blood cells exposed to electrospun nanofibrous matrix. PC: Positive control; NC: Negative control; (A) GP, (B) GP-$(L\text{-}AgSD)_5$, (C) GP-$(L\text{-}AgSD)_{25}$ and (D) GP-$(L\text{-}AgSD)_{50}$, [b] Hemolytic activity of electrospun nanofibrous matrix, [c] *In vitro* biocompatibility of NIH 3T3 fibroblasts cells on 6, 24, 72 and 168 h using MTT assay, [d] Calcein AM-DAPI fluorescence staining images of NIH 3T3 fibroblasts' cell adherence and proliferation onto GP-$(L\text{-}AgSD)_{25}$ nanofibrous matrix at 6, 24, 72 and 168 h. The scale bar is 75 µm

Figure 6 Optical photographs depicting the progress of wound healing till 20 days

Figure 7 [a] Quantitative wound closure rate of control and treated groups, [b] Comparison of variations in body weight of control and treated groups. $*P< 0.05$ compared between day 0, 4, 8 and 12 of group 1 and 2; day 0, 4, 8, 12 and 16 of group 3 and 4; $*P< 0.05$ compared between day 0 and 12 of group 6; # $P< 0.01$ compared between day 0 and day 16 of group 5; day 0 and 4 of group 7. [c] Tensile strength of healed wound tissues of control and treated groups. $*P< 0.05$ compared with group 7; $**P< 0.01$ compared with group 7; $***$ $P< 0.001$ compared with group 7; # $P< 0.05$ compared with group 2. [d] Elongation at break of healed wound tissues of control and treated groups. $*$ $P< 0.05$ compared between group 1 and 7, 2 and 3, 3 and 6;♦ $P< 0.01$ compared with group 7; # $P< 0.001$ compared with group 7. [e] Effect of the nanofibrous matrix

on the hydroxyproline content. ∗P< 0.01 compared with day 4 and 12 in group 1, to 6 except group 2; ∗P< 0.01 compared with day 4 and 16 in group 1, 2 and 6; ∗P< 0.01 compared with day 8 and 12 in group 3; ∗P< 0.01 compared with day 8 and 16 in group 1and 7. [f] Effect of the nanofibrous matrix on the hexosamine content. ∗P< 0.05 compared with day 4 and day 12 in the non-infected group; ∗P< 0.05 compared with day 4 and day 12 in the Silvadene® treated group

Figure 8 H&E images of control and treated groups on 4^{th} (A, C, E, G) and 16^{th} day (B, D, F, H) post wounding; MT images of control and treated groups on 4^{th} (I, K, M, O) and 16^{th} day (J, L, N, P) post wounding (magnification: 40×). Group 1: Non-infected control, group 2: Infected control, group 3: GP-(L-AgSD), group 7: Silvadene®. N, C, E, WM and HF refers to the neutrophils, collagen, epidermis, wound margin and hair follicle respectively. The scale bar is 100 µm

Figure 9 Immunohistochemical staining for MMP 2, MMP9 and TNFα post-burn days. The scale bar is 340 µm

Durable nanofibrous matrices augmented with hydrotalcite-like compounds for cutaneous regeneration of burn wounds

Vimala Devi Mohan[a], Liji Sobhana S. S.[c], Punalur John Shiny[a], Giriprasath Ramanathan[a,d], Grace Felciya Sekar Jeyakumar[a], Velswamy Poornima[a], Sathiah Thennarasu[b], Pedro Fardim[c,d,*], Uma Tiruchirapalli Sivagnanam[a,*]

[a]*Biological Materials Laboratory, CSIR-Central Leather Research Institute (CLRI), Adyar, Chennai, India*

[b]*Organic Chemistry Division, CSIR-Central Leather Research Institute (CLRI), Adyar, Chennai, India*

[c]*Laboratory of Fiber and Cellulose Technology, Abo Akademi University, Porthansgatan 3, FI-20500 Abo, Finland*

[d]*Chemical Engineering for Health & Care, Bio&Chemical Systems Technology, Reactor Engineering and Safety, Department of Chemical Engineering, KU Leuven, Celestijnenlaan 200F bus 2424, B-3001 Leuven, Belgium*

*** Corresponding authors email addresses:**

Dr. Uma Tiruchirapalli Sivagnanam (suma67@gmail.com),

Prof. Pedro Fardim (pfardim@abo.fi; pedro.fardim@kuleuven.be**)**

1. Introduction

Skin, the major organ of our body, functions to regulate the body temperature and protects us from external harmful factors. The chances of microbial infection and its associated risks are high in a damaged skin. This is inevitable to promote healing and reduce infection. Current challenges in wound care management include inadequate delivery of drug, poor contact between drug and the wound and irregular deposition of antimicrobial agents at the wound site. However, these limitations are addressed with the development of wound dressings, which can be applied as a protective cover over the injured site (Martin et al., 2013).

The development of wound dressing material began with the need of a physical barrier to prevent microbial infection and accelerate healing. The characteristic features of wound dressing material include absorption of wound exudates, inhibit microbial entry at wound site and enhance the aesthetics of skin. Previous studies clearly exhibits the various forms of dressings available in the market such as sponges (Dai et al., 2009), hydrogels (Ouyang et al., 2018), foams (Timmers et al., 2008) and films (O'Brien, 2011), which primarily contains hydrocolloids, alginates and composites. In addition, two-dimensional nanofibrous matrix are extensively preferred due to its high surface to volume ratio, oxygen permeability and biocompatibility (Garg et al., 2012). Nanofibrous matrix are yet another form of film-based dressing that mimic the function of natural extracellular matrix and serve as a suitable environment for cell attachment and proliferation (Smith and Ma, 2004; Unnithan et al., 2012). The current work explores the possibility of constructing a nanofibrous matrix with dual action of antimicrobial activity followed by wound healing through a drug propelled carrier system.

The use of layered double hydroxides (LDH) as a drug carrier, apart from its conventional use as catalysts, adsorbents, and environmental remediation materials has earned the interest of

scientists (Williams et al., 2006; Qiu and Hou, 2009; Jin et al., 2010; L. Sobhana et al., 2016; Liji et al., 2016; S. S. L. Sobhana et al., 2016; Sobhana et al., 2017). As the name suggests, they are a class of ionic lamellar compounds that are made of unique positively charged brucite-like layers in which partial substitution of the divalent cations with trivalent ions give rise to positively charged sheets counter balanced by anionic species. Several reports have documented the efficacy of these hydrotalcite-like materials as carrier molecules (Shafiei et al., 2015; Ge et al., 2016). Owing to these interesting properties, the current study proposes to immobilize a drug on the surfaces of LDH particles. Many therapeutic molecules such as peptides, proteins and natural organic molecules are negatively charged at neutral to near neutral pH values. Hence, they tend to interact strongly with materials like LDH having positive charges. Thus, the drug carrying ability of LDH can be extrapolated to wide range of drugs for medical applications.

Several antiseptic agents such as povidone-iodine, alcohol, chlorhexidine and honey are topically used for the treatment of burn wounds (Andreu et al., 2015). Burn wounds are prone to bacterial growth and infection (Jahromi et al., 2018). Silver-based dressing material still seems to be the finest of choice for treating burn wound injuries and infections (Shanmugasundaram et al., 2009; Heo et al., 2013; Shao et al., 2017). However, the bioavailability of the drug delivered through cream based formulation is very low due to wash out with the exudates and lower absorption resulting in frequent dressing changes that would traumatize the new epithelial surface resulting in delayed wound healing (Sano et al., 1982).

The conventional methods used for the fabrication of matrix including that of phase separation (Budyanto et al., 2009), extrusion (Kim et al., 2014), gas foaming (Jiang et al., 2015) and template synthesis (Martín et al., 2012) suffer certain drawbacks such as use of only compatible polymers, stability concerns on drug and polymer, poor pore interconnectivity, need for post-

synthesis process to remove the templates, etc. In order to overcome these drawbacks, an attempt was made to fabricate the nanofibrous matrix by electrospinning. The process of electrospinning offers various advantages such as ease of operation using wide range of polymers, cost-effective and yields nanofibers of high surface to volume ratio (Nagiah et al., 2013b).

In the present study, AgSD loaded LDH has been electrospun along with polymers to yield a therapeutic hybrid matrix. Nonetheless, the soluble form of silver is biologically active against microbes. Moreover, the AgSD dissociates in solution to form cationic silver ions and anionic sulfadiazine molecules to impart antibacterial property at the wound site. Gelatin (G), the renewable bio-protein was chosen due to its excellent biocompatibility, and adhesiveness (Nagiah et al., 2013a, 2013b; Rathore et al., 2016) However, gelatin as such cannot be electrospun due to its poor fiber-forming ability and mechanical stability. Hence, it has to be often blended with other polymers to obtain nanofiber through electrospinning (Fallah et al., 2016). Herein, Poly-3-hydroxybutyric acid (P), a biodegradable common metabolite present in all higher living organisms, which proves its non-toxicity was chosen for the fabrication of the scaffold (Matrix) (Nagiah et al., 2013b).

Furthermore, an attempt was made to deliver AgSD in a controlled fashion on the target site with the help of the fabricated carrier material, LDH. Moreover, the knowledge from our works indicate, that the electrospinning of G and P as a nanofibrous matrix (Nagiah et al., 2013b), collagen coated (Ramanathan et al., 2016) and dual layered (Singaravelu et al., 2017) nanofibrous scaffold act as a promising material for excision type wound healing. Nevertheless, the polymers G and P act as a substrate for cell adhesion, proliferation, complete re-epithelialization and synthesis of collagen in wound healing process. Based on these results, G and P were chosen as a matrix to deliver AgSD adsorbed on LDH to accelerate healing of burn

wounds. Thus, the fabricated GP-(L-AgSD)$_n$ matrix was studied thoroughly for its physicochemical, drug release behavior, biological and mechanical properties as a biomaterial in tissue engineering application. The *in vivo* wound healing ability of the electrospun nanofibrous matrix was assessed by using male Wistar rats to assess the rate of wound closure.

2. Experimental Methods

The experimental methods to synthesis Mg:Al LDH, drug adsorption on LDH and drug loading efficiency on LDH was well explained in the supplementary information.

2. 1. Electrospinning of nanofiber matrices with L-AgSD hybrid

Equal concentrations of G and P were prepared by dissolving them separately in HFIP under constant stirring (4 wt/vol%). To achieve an optimum drug release from the electrospun matrix for effective inhibition against infection at the wound site, various quantities of L-AgSD namely 5, 25 and 50 mg was added to 5 mL of the polymer solution containing G:P in the ratio 30:70 for spinning (Nagiah et al., 2013b). After electrospinning, the electrospun samples were named as GP-(L-AgSD)$_n$ where n is the mass of L-AgSD in milligrams added to 5 mL of the polymer solution. The detailed experimental part was well explained in the supplementary information.

2. 2. Characterization studies of the L-AgSD hybrid and GP-(L-AgSD)$_n$ nanofibrous matrix

All the Characterization methods like X-ray diffraction pattern, Fourier transform infrared (FTIR) spectrum, Thermo gravimetric analysis (TGA), High Resolution Scanning Electron Microscopy (HR-SEM), Atomic Force Microscopy (AFM), and Contact angle was performed in this study was well explained in the supplementary information. The porosity (Jithendra et al., 2013) and swelling index (Taepaiboon et al., 2006) of the nanofibrous matrix was investigated. The detailed experimental part was well explained in the supplementary information. The mechanical property of the all the nanofibrous matrices were analyzed by cutting the nanofibrous

matrices into dumb-bell shaped specimens (100 x 16 mm^2), and the load–elongation measurement was measured using a universal testing machine (INSTRON model 1405) according to Vogel at an extension rate of 5 mm/min (Muthukumar et al., 2014). The rate of degradation of the nanofibrous matrix was determined by using collagenase enzyme (Zhong et al., 2007). The *in vitro* release pattern was studied for all the three formulations using Franz diffusion apparatus (Chakraborti et al., 2012). The antibacterial inhibition test (Xing et al., 2010) and in vitro bacterial viability assay (Arakha et al., 2015) was performed to the nanofibrous matrix. The detailed experimental part was well explained in the supplementary information. The Hemocompatibility assay (Vatankhah et al., 2014) was carried out to determine whether these nanofibrous matrices are hemocompatible with fresh blood when used for *in vivo* application. The MTT assay, cell attachment and proliferation were performed to assess the cell viability of the electrospun nanofibrous matrix using NIH 3T3 fibroblast cell line (Ramanathan et al., 2016). The detailed experimental part was well explained in the supplementary information.

2. 3. In vivo animal studies: Burn wound model

Eighty-four male Albino Wistar rats weighing 190-220 g were individually housed in temperature and humidity-controlled room, monitored continuously with feed and water *ad libitum*. They were randomly divided into seven groups with twelve animals in each group (Non-infected control, infected control, GP-$(L\text{-}AgSD)_{25}$, GP, GP-AgSD, GP-L, standard formulation Silvadene® cream). Three animals were sacrificed from each group at regular intervals. The Institutional Animal Ethics Committee (IAEC) approved the experimental protocols that were performed.

2. 3. 1. Experimental design

A temperature-controlled soldering rod attached with a circular iron disc of 10 mm diameter was used to impose second-degree burn injury on rat models (Shanmugasundaram et al., 2009). The disc was preheated to 82°C-86°C and allowed to stand for 20 minutes to stabilize the temperature. It was then placed over the shaved and disinfected dorsal side of the rats for 20 seconds without applying any external pressure. Before creation of the burn wounds, all the rats were initially anaesthetized using thiopental sodium (22-24 mg/kg body weight).

Fig. 1[a] shows the induction of burn wound in rat. The γ-ray sterilized electrospun matrix was cut into 1.5 cm x 1.5 cm and placed on the surface of the wound using sterile forceps. For the experimental control (group 1 and 2), sterile cotton gauze was placed on the wound site. The wound dressing material was changed periodically at an interval of 4 days (4^{th}, 8^{th}, 12^{th}, 16^{th} day) and three rats in each group were euthanized to collect the granulation tissue.

The induction of microbial infection (Grzybowski et al., 1999), wound healing assessment and estimation of hydroxyproline and hexosamine content in the granulation tissues were determined by the method of Woessner (J. Woessner, 1961), and Elson and Morgan (Elson and Morgan, 1933) respectively. Moreover, the assessment of regulatory cytokines during the *in vivo* studies were performed for the expression of inflammatory cytokines like TNFα, MMP2 and MMP9**.** The detailed experimental part was well explained in the supplementary information.

2. 4. Statistical analysis

All statistical evaluations were carried out using Graph Pad Prism 5 software (Graph Pad Software, San Diego, CA). The results were expressed as mean ± SEM. Statistically significant differences (*P*) were analyzed either by a one or two-way ANOVA with Tukey's post-hoc testing. A value of $P < 0.05$ was statistically significant.

3. Results and discussion

For the easy understanding of the readers, first the characterization results for L-AgSD hybrid material had been discussed, followed by the results for GP-(L-AgSD)$_n$ electrospun nanofibrous matrix.

3. 1. L-AgSD hybrid characterization

3. 1. 1. XRD analysis

The XRD spectra of the composite were given in **Fig. 1[c]** and structure of AgSD was depicted in **Fig. 1[b]**. LDH (Mg:Al) exhibits the pattern of typical crystalline hydrotalcite phase (JCPDS no. 14-0191) which has hexagonal lattice with rhombohedral symmetry and layered features. The main characteristic reflection of L-AgSD hybrid centered at 11.5°, 23.2° and 34.7° can be indexed to (003), (006) and (009) planes of Mg:Al LDH (S. S. L. Sobhana et al., 2016) and the reflections at 8.9°, 10.3° and 18.6° are ascribed to (002), (011) and (020) planes of AgSD which indicates the intrinsic structure of AgSD. The diffraction pattern further reveals that the drug AgSD has occupied the brucite layers by adsorption rather occupying the interlayers of the heterostructure. This was confirmed by the pattern exhibited by L-AgSD where the 003 reflection does not show any shift when compared to the reference LDH and AgSD. Thus, the method for the synthesis was carefully chosen to attain crystallinity for better adsorption of our targeted drug on the cationic layers for further wound healing applications. The pattern also clearly reveals that there was no formation of any secondary phases or impure phases in the form of MgO which might form during the aging process (Klemkaite et al., 2011). Therefore, the co-precipitation method adopted for synthesis has greatly favored the formation of phase pure Mg:Al LDH. Adsorption was more predominant since there was no shift in the diffraction pattern of the final hybrid material compared to LDH alone.

3. 1. 2. FTIR analysis

The adsorption of AgSD on LDH was verified by mid-infrared spectroscopy. **Fig. 1[d]** shows the FTIR spectra of LDH, AgSD, and L-AgSD respectively. The broad absorption band at 3492 cm^{-1} corresponds to the stretching of –OH groups in the brucite-like layer and physiosorbed water.(Pan et al., 2010) For pure AgSD, the band at 1596 cm^{-1} was assigned to vibrational stretching of its phenyl structure conjugated to the NH_2 group (Chakavala et al., 2012; El-feky et al., 2017), the band at 1656 cm^{-1} attributed to NH_2 bending (El-feky et al., 2017) and the band at 1352 cm^{-1} was ascribed to the asymmetrical stretching of the S=O bonding (Chakavala et al., 2012; Li et al., 2015). The structural evaluation of the material before and after treating LDH with AgSD drug reveals that pristine Mg:Al LDH has carbonate groups in the site of intercalation between the layers. The precursors used for the synthesis of this material were nitrate based salts but the FTIR spectrum shows that the intercalated anion was carbonate which clearly shows that carbonate has the highest tendency to enter the galleries of LDH than any other anions. The weak band at 1624 cm^{-1} is due to the water deformation mode. A series of bands recorded in the low wavenumber region can be ascribed to Mg:Al-OH, Al-OH translation modes and Al-OH deformation. All these observations indicate the adsorption of AgSD on LDH.

3. 1. 3. Thermal analysis

The thermogram of LDH (**Fig. 1[e])** shows a gradual mass loss till 224°C which may be attributed to the loss of adsorbed water molecules and those found in the interlayers of the LDH lamellae. The mass loss continues as the temperature increases from 225 to 500°C which corresponds to the loss of hydroxyl groups from the brucite like layer along with the release of interlayer carbonate anions resulting in the formation of mixed metal oxides with disrupted layered structure. The mass loss of this region was also attributed to the loss of water and CO_2

through slow decomposition of the inorganic phases after the disruption of the hydrotalcite. A similar trend has been reported for MgAl LDH intercalated with carbonate anions (Klemkaite et al., 2011) and ZnAl LDH synthesized using cellulose as a biotemplate (S. S. L. Sobhana et al., 2016). In the case of AgSD, the first decomposition occurs from 283 to 329°C which can be attributed to aminopyrimidine decomposition. The second mass loss observed from 420 to 650°C can be assigned to the aromatic ring and sulfur dioxide decomposition and the profile obtained highly correlates with the trend obtained for AgSD containing corn starch and cellulose extrudate matrix (Zepon et al., 2014). From the thermogram, it is evident that there is no significant change in mass loss between free drug and AgSD adsorbed on LDH. However, when the developed scaffold is applied as a burn wound dressing, the drug present in the composite will remain stable at an average body temperature.

3. 1. 4. Particle size distribution and zeta potential

The particle size distribution and zeta potential of LDH and AgSD adsorbed LDH were measured using dynamic light scattering analysis. The hydrodynamic diameter (Z_{av}) of LDH was 258 nm and the calculated polydispersity index (PDI) was 0.212 which was indicative of monodispersed size distribution **(Fig. 1[f])**. On adsorption of AgSD, the resultant L-AgSD nanohybrid powder showed marginal increase in the average particle size (Z_{av}) to 380 nm and PDI of 0.08. The zeta potential of as-synthesized LDH was +30.7 mV denoting a moderately stable suspension which is attributed to the positively charged layers of LDH. A study reported by Fang et al. had discussed the pH-dependent surface charge of MgAl LDH wherein ζ in the range of +30 to +40 mV was obtained for pH 7-8 and it corroborates well with our observation (Fang et al., 2015). The electrokinetic potential of L-AgSD hybrid was obtained to be -45.2 mV which implies an equilibrium binding of drug molecules onto the surface of LDH yielding a

more stable suspension. A stable complex of LDH-MTX was prepared which displayed a zeta potential of +36.3 mV which falls well within the stable range (Chakraborty et al., 2013).

3. 1. 5. Morphology analysis using SEM

Microscopic image of as-synthesized Mg:Al LDH are composed of a large number of typical flat hexagonal plate-like crystals (**Fig. 2[a]**) Similar hexagonal plate-like structures were reported for MgAl LDH by Gu et al. (Gu et al., 2008) and Shafiei et al (Shafiei et al., 2016). The chemical composition of pristine LDH determined by elemental analysis revealed that the ratio of metal ions was 2:1 (**Fig. 2[b]**). The hybrid L-AgSD shows a cloudy appearance of the drug being adsorbed on the surface of LDH. The flaky structure of LDH was not hampered during the formation of L-AgSD hybrids (**Fig. 2[c]**). This type of structure was anticipated in our study for the purpose of drug release from the matrix to the wound site. The L-AgSD hybrid shows the presence of Ag and S peaks arising from AgSD in the hybrid material (**Fig. 2[d]**).

3. 2. Characterization of the electrospun nanofibrous matrix

3. 2. 1. XRD analysis

The X-ray diffraction patterns were analyzed for all matrices to investigate its crystalline structure as reported in **Fig. 2[e]**. The X-ray diffraction pattern of all the nanofibrous matrices show a broad gelatin reflection at 22° and a sharp reflection at approximately 13° attributing to the crystalline nature of poly-(3-hydroxybutyric) acid **(Fig. 2[e](A)).** A control matrix loaded only with AgSD shows the characteristic reflection of AgSD (**Fig. 2[e](B)**). Both the drug and the polymer present higher crystallinity than LDH, which can avoid the visualization of LDH peaks (Fig. 2[e](C-F)). However, this lower structural order of LDH had resulted in its successive dispersion into the nanofibrous matrix. A study on LDH/AMOX incorporated into

PCL nanofibers shows that the nanohybrid has distorted layers of hydroxides upon drug incorporation, thereby enabling its uniform distribution (Valarezo et al., 2013a).

3. 2. 2. Thermal analysis

Thermogravimetric analysis was performed for all the nanofibrous matrices. A three-step mass loss was observed for all samples. The first mass loss observed between 30 and 95°C corresponding to the loss of moisture from gelatin was higher for increasing composition of L-AgSD complex as shown from $T_{-5\%}$ values in **Fig. 2[f]**. Naveen et al. had obtained a similar thermal degradation pattern for Gel-PHB nanofibers (Nagiah et al., 2013b). The second mass loss occurring between 200 and 270°C arises from the dehydroxylation of the layers of LDH. The various amounts of L-AgSD in the nanofibrous matrix did not produce a further relevant decrease in the melting peak (T_m) as shown in **Table S1**. As the temperature approached 800°C, it was observed that 20% of matrix loaded with 25 and 50 mg of L-AgSD still remained as residue whereas the matrix with lowest L-AgSD complex and without the drug was almost thermally decomposed completely. Thus, the incorporation of L-AgSD complex had imparted thermal stability to the polymeric nanofibrous matrix.

3. 2. 3. Morphology analysis using SEM

The surface morphology of the nanofibrous matrices were analyzed using HR-SEM. **Fig. 3[a]** and **Fig. 3[b]** depicts that these nanofibers are randomly oriented and possess a bead-free well interconnected network structure. The L-AgSD particles were seen embedded on the fibers in the concentration studied and was distributed throughout the entire electrospun nanofibrous matrices (Qing Qin, Ya Liu, Si-Chong Chen, Fei-Yu Zhai, Xin-Ke Jing, 2012). The diameter of GP nanofibers ranges from 120-140 nm and those of L-AgSD impregnated electrospun nanofibrous

matrix were also apparently the same. The microscopic images of the nanofibrous matrix also exhibited a porous structure which was later confirmed by a higher swelling index.

3. 2. 4. Atomic force microscopy

Fig. 3([A-D]) shows the 3D topographic surfaces of the electrospun matrices. The surface roughness was determined using Gwyddion AFM data processing software. The microtopographic images reveal rigidity and discrete altitude variations. It was determined to be 29.51 ± 3.25 nm for matrix containing GP and the roughness gradually increased as the ratio of L-AgSD incorporation into the polymer matrix increased. The values were calculated to be 31.24 ± 2.73 nm, 36.06 ± 3.20 nm and 40.03 ± 1.86 nm for matrix having 5, 25 and 50 mg of L-AgSD respectively. Parvinzadeh et al. had reported that the surface roughness of poly ethylene terephthalate based nanocomposites increases by the addition of modified nanoclays (Parvinzadeh et al., 2010). Manikandan et al. had showed that roughness of polyurethane nanocomposite was enhanced by incorporation of murivenna oil favoring hemocompatibility (Manikandan et al., 2017). This result suggests this type of microenvironment to be a suitable surface for cell adhesion.

3. 2. 5. Porosity

The diffusion of gases, metabolite, nutrients and molecular signals between the matrix and the surrounding system makes the nanofibrous matrix more susceptible to mimic the nature of the ECM architecture for cell penetration and proliferation. Thus, porosity plays a critical parameter for nanofibrous matrix. As the concentration of L-AgSD complex increases in the nanofibrous matrix, the porosity seems to gradually decrease (**Fig. 4[a]**). The porosities were 71.5% for GP, 69.4%, 66.8% and 64.3% for matrix with containing 5, 25 and 50 mg of L-AgSD respectively. Moreover, the obtained porosity was more adequate for a wound dressing material to promote

moisture and oxygen exchange. Chandrasekaran et al., has reported with poly(L-lactic acid)-co-poly(ε-caprolactone) nanofibers with a porosity of 84% has been suitable biomaterial in skin regeneration (Chandrasekaran et al., 2011).

3. 2. 6. Contact angle measurement

The surface wettability of a biomaterial will affect cell adhesion, migration, and proliferation of cells (Lin et al., 2012; Liu et al., 2017). For this reason, the water contact angles of all electrospun matrices were determined as shown in **Fig. 4[b]**. As expected, the matrix containing a blend of polymers is more hydrophilic in nature with a contact angle of 60.35°. Moreover, the extent of wettability decreased as the ratio of L-AgSD content increased in the electrospun nanofibrous matrix and it was determined to be 69.62°, 75.31° and 89.62° for 5, 25 and 50 mg respectively. This reduction in hydrophilicity was attributed to the well-known fact that the L-AgSD complex was hydrophobic and hence hinders the extent of wettability. Thus, it was confirmed that the developed matrix has the desired hydrophilicity as a wound dressing material. It is a pre-requisite for any scaffold to be hydrophilic so that it enhances the ability of cells to adhere, proliferate and absorb wound exudates. A study on the composite scaffold using polylactic acid m(PLA) and a biodegradable elastomer, poly (1, 8-octanediol-co-citric acid) also found that the hydrophilic nature of the scaffold was found to be in the range of 99 to 139° (Zou et al., 2019). These studies emphasize the importance of hydrophilicity as a vital factor in the design of a wound dressing material.

3. 2. 7. Swelling index

The determination of the swelling index of the nanofibrous matrix is more important to predict its exudate management and is a vital factor that controls the release of the loaded drug. **Fig. 4[c]** reveals that the swelling percentage of all the matrices lies between 200 and 260% and was

inversely proportional to the L-AgSD complex present in the nanofibrous matrix. It was observed that both the GP containing matrix and that loaded with 5 mg L-AgSD complex reached the swelling saturation after 54 h whereas it was 48 h for higher concentrations of the nanohybrid complex. Xu *et al.* have reported a swelling index of 240% for chitosan/silk microfibers which maintains the necessary conditions for wound healing (Xu et al., 2015). These findings suggest that the fabricated matrix was suitable for tissue engineering application.

3. 2. 8. Mechanical testing

The mechanical properties of the nanofibrous matrices which were designed for direct human application need to be robust enough for both handling and sterilization. **Table 1** exhibited a gradual increase in the tensile strength with increase in the concentration of L-AgSD complexes in the nanofibrous matrix. The mean tensile strength of only the polymeric matrix was 3.12 ± 0.10 MPa and the matrix loaded with 25 mg L-AgSD was 5.32 ± 0.14 MPa. Elongation at break denotes the flexibility of a fabricated material. Increase of L-AgSD had no significant effect on the percentage elongation at break. Mechanical strength analysis of the co-electrospun collagen and zein indicates that the tensile strength of the fabricated material increased with respect to zein concentration (Lin et al., 2012). A similar trend of increase in strength was observed with increasing concentrations of L-AgSD. Shafiei et al. have also reported that the tensile strength of the polymer alone was found to be 1.63 MPa while upon addition of the nanoclay the tensile strength increased to 1.996 MPa (Shafiei et al., 2016). The results obtained and these reports suggest that the nanoclay might influence the stretchability and the tensile strength of the scaffold on a whole.

3. 2. 9. In vitro degradation behavior

The degradation rate and the biological stability of the nanofibrous matrix was evaluated using collagenase enzyme. **Fig. 4[d]** shows that the polymeric nanofibrous matrix exhibited 63.5% mass loss and matrix containing L-AgSD showed 44.8%, 47.9% and 47.6% mass loss with increase in concentration of the drug bound LDH respectively. Accounting to the importance of any biomaterial, biodegradability was an important factor to be considered. An exclusive study on degradation of silk fibroin sheets by several enzymes have been carried out where the degradation rate was determined to be approximately 70% (Li et al., 2003). This signifies the importance of any biomaterial to act as a substrate for proteolytic degradation.

3. 2. 10. In vitro drug release assay

The *in vitro* drug release kinetics of AgSD bound to LDH from the nanofibrous matrices were assessed to investigate the release profile, depending on the controlling parameters *viz.*, drug concentration, fiber diameter and location of the drug with respect to fibers (Valarezo et al., 2013b). The cumulative percentage of AgSD release with respect to time is plotted in **Fig. 4[e]**. After 4 h around 48%, 50% and 56% of AgSD was released from 5, 25 and 50 mg of L-AgSD loaded nanofibrous matrices respectively. This initial burst release of approximately 50% of the drug was desirable and mandatory because any medication intended to control infection at the wound site must exhibit immediate preventive action (chemoprophylaxis) followed by a controlled release up to 72 h. There was a remarkable increase in drug released between 4-12 h after which equilibrium concentration was achieved and maintained till 72 h. In the case of nanofibrous matrix loaded with 50 mg L-AgSD, almost all the drug was released within 72 h. For nanofibrous matrix loaded with 5 and 25 mg L-AgSD, 75% and 86% of the drug had been released over a period of 72 h in a controlled fashion. The nanofibrous matrix with 25 mg L-AgSD released-ptimum measure of drug to combat infection was confirmed by the antimicrobial

studies, which meets the requirements for use as a dressing material. Hence, the scaffold GP-(L-AgSD)$_{25}$ was used for further experiments. Moreover, to prove the need for a carrier molecule to release the drug, the release profile of AgSD from GP-(L-AgSD)$_{25}$ was compared with that of the free drug embedded in the polymeric matrix as illustrated in **Fig. 4[f]**. It was observed that 86% of AgSD had been released in 72 h from the clay nano-hybrid loaded into the matrix compared to the complete release of free drug from the matrix in a short span of time. This difference in release behavior indicates the vital role of LDH as an efficient drug carrier moiety. From these results, it was found that by incorporating AgSD in LDH-polymer film formulations, the antimicrobial activity can be extended over longer durations; a major advantage for a drug eluting wound dressing material.

3. 2. 11. Antibacterial Inhibition and Live/Dead studies

For a wound dressing material to be efficient, the nanofibrous matrix loaded with L-AgSD complex should inhibit the growth of bacterial infection at the wound site. The gradual release of AgSD from the nanofibrous matrix resulted in excellent inhibitory activity against each organism. The scaffold exhibited a MIC and MBC of 48.4 and 52.8 µg/mL against *P. aeruginosa* while *S. aureus* exhibited it as 60.6 and 66.4 µg/mL respectively. Moreover, the viability of the GP-(L-AgSD)$_{25}$ matrix treated against *P. aeruginosa* was further tested using LIVE/DEAD viability assay containing nucleic acid binding dyes. The untreated bacterial cells (**Fig. 4[A]**) were viable and healthy, exhibiting green fluorescence (Arakha et al., 2015). The cells treated with the matrix showed a significant reduction in cell viability as shown in **Fig. 4[B]**. This observation confirms the fact that silver ions from the drug SSD bind to the membrane and disrupt the cellular integrity. This results in the leakage of proteins, disruption of folic acid mechanism, and thereby cell death.

3. 2. 12. In vitro biocompatibility studies

3. 2. 12. 1. Hemolysis assay

Hemocompatiblity was an essential property for a matrix being intended for tissue engineering application. Therefore, any material that induces hemolysis cannot be suitable for wound healing purposes. Our fabricated nanofibrous matrices exhibited no visible signs of hemolysis, compared to the positive control shown in **Fig. 5[a]**. According to standards, samples exhibiting less than 5% are considered to be non-hemolytic (Chen et al., 2008) and the same can be observed in **Fig. 5[b]** which suggests that all electrospun matrices containing varying ratios of L-AgSD were hemocompatible in nature.

3. 2. 12. 2. Co-culturing fibroblasts with electrospun nanofibrous matrix

The biocompatibility of the nanofibrous matrix was determined using MTT assay. The percentage cell viability of the matrices with NIH 3T3 fibroblast cells after 1, 2, 3 and 7 days was exhibited in **Fig. 5[c]**. The cell adhesion and proliferation over the nanofibrous matrix plays aids the construction of the ECM matrix, which will enhance the uniform spreading of cells and healing of wound. The nanofibrous matrix was found to be highly compatible and non-toxic with relative cell viability greater than 90%. Interestingly, with increasing time, more cells proliferated on the matrix which was observed as a significant increase in cell viability. Nonetheless, this proves that these matrices are biocompatible with the presence of LDH and AgSD. *In vitro* fluorescent behavior of the cells over the nanofibrous matrix is depicted in **Fig. 5[d]**. The nanofibrous matrix forms the backbone for the cell adhesion and proliferation. The nanofibrous matrix with 25 mg L-AgSD demonstrated adequate cell adhesion that initiates effective wound healing (Singaravelu et al., 2016). The scaffolds made with PCL-LDH were found to have more viable cells growing on the fibrous matrix (Shafiei et al., 2016). The surface

topography enabled higher percentage of cell adhesion and proliferation. Several studies also suggest that the hybrid with nanoclay had a positive impact on the cell behavior, colonization and the proliferation of the cells (Akhilesh K. Gaharwar et al., 2014). The electrospun gelatin and PHB was found to support dermal keratinocytes and fibroblasts as reported by Nagiah et al. (Nagiah et al., 2013a). All these studies show that the matrix shows good biocompatibility as observed in our study.

3. 2. 13. Progression of wound healing by the nanofibrous matrix

The *in vivo* wound healing efficacy of the nanofibrous matrix was determined by placing the material on the burn wounds. The matrices when placed on the wound site, adhered effortlessly owing to the hydrophilic nature of the polymers which provided adequate moisture and flexibility for application. No mortality was observed throughout the course of experiment. Over the course of wound healing the granulation tissue was collected, and the body weight of the animals was recorded. Influence of the matrix on wound closure at different time points as confirmed by macroscopic analysis is depicted in **Fig. 6**. Similar observations like the rate of wound contraction, biochemical analysis and histological examinations were performed to evaluate the wound healing activity by Mazlyzam et al (AL et al., 2015).

The quantitative wound closure rate was determined by tracing the perimeter of the wound onto a graph sheet at specified time intervals as represented in **Fig. 7[a]**. The group treated with Silvadene® achieved higher wound closure rate of 98 ± 5.8% on day 20. The wound closure rate for the other groups as observed on the twentieth day post-wounding was found to be in the following order: GP-(L-AgSD)$_{25}$ (95 ± 7.3%), GP-AgSD (93 ± 8.2%), GP (88 ± 5.9%), Non-infected control (81 ± 6.8%), GP-L (71 ± 6.2%), infected control (63 ± 4.6%).

435 ***3. 2. 14. Body weight assessment***

436 The average body weight of the rats was 207 g. All the control and experimental rats were
437 monitored throughout the study period and body weight was measured and expressed as mean ±
438 standard error (**Fig. 7[b]**). For the animals treated with Silvadene®, there was an initial decrease
439 in the body weight after inducing wound. As the healing of wound progressed, the animals
440 regained their weight. The control and treated groups showed a reduction in body weight on the
441 4^{th} day post wounding but showed no significant difference from day 16 as the wound healed.

442 ***3. 2. 15. Mechanical properties of the granulation tissue***

443 To evaluate the mechanical strength of the newly formed granulation tissue, the tensile strength
444 and % elongation at break was measured. The tissues collected from the euthanized rats at day
445 20 were cut into lengthwise strips of 3 cm width such that the induced wound area lies at the
446 centre. The tensile strength and elongation at break of all the control and experimental groups
447 were shown in **Fig. 7[c]** and **Fig. 7[d]** respectively. The tensile strength was found to be higher
448 corresponding to the rate of proliferation of cells. The higher tensile strength can be corroborated
449 to the faster rate of wound healing in the groups 3, 5 and 7 which might be due to collagen
450 deposition and re-epithelialization (Choi et al., 2018).

451 ***3. 2. 16. Histological examination***

452 The granulation tissue samples were stored in buffered formalin and then stained with
453 haematoxylin and eosin (H&E) as well as Masson's trichome (MT) staining. Paraffin sections of
454 the samples were prepared and examined using light microscopy to evaluate the level of
455 granulation tissue formation and wound re-epithelialization. The burn had resulted in the loss of
456 follicles that are deep in the dermal section. According to the histological figures (**Fig. 8**), the
457 sections of group 3 treated with GP-(L-AgSD) showed minimal necrosis compared to the control

groups. Granulation was initiated after the formation of crest on day 2 in all the groups. The rate of re-epithelialization was similar in groups 3 and 7 when compared to the groups 1 and 2 which showed a lower rate of epithelialization. The sections from the control group show the presence of neutrophils and macrophages indicating an inflammatory response. The infiltration of white cells was found to be decreasing in the Silvadene® treated group. On day 12, neoepidermis formation was observed in group 3 and 7, whereas the control groups had a large open wound area. Towards day 16 a normal pattern of hair growth was observed in the area surrounding the wound site with a thicker epidermis and a good extent of collagen deposition. Restrained healing and a thin epidermal layer are observed in the control group due to microbial load. These results suggest that the controlled release of the drug in the group treated with the complete matrix has successfully controlled the infection and accelerated wound healing.

Masson's trichrome staining was used to study the collagen deposition at the wound site. The deposition of collagen is proportional to the strength and the healing of the wound. On day 12 of group 3 and 7, a pronounced deposition of collagen is observed with densely packed fibers. Well-oriented collagen was seen to be deposited with a thicker granulation tissue in the GP-(L-AgSD)$_{25}$ and Silvadene® treated groups. Uniform distribution of collagen is observed in corroboration with the decreased level of hexosamine as discussed below.

3. 2. 17. Biochemical analysis

The estimation of hydroxyproline was vital in understanding the collagen turnover post-wounding. Collagen was an integral part of the extracellular protein that was present in the granulation tissue. An increase in the level of hydroxyproline indicates an accelerated wound healing as shown in **Fig. 7[e]**. Both the treated and control groups showed a lower hydroxyproline level at day 4 post-wounding. It was also observed that the amino acid content

was at its peak at day 8 which later reduced as the wound healing progressed for Silvadene® treated groups. For group 3, the level was higher at day 12 which aids in rapid healing. On the contrary, the control groups showed an increased collagen content at day 16 which attributes to delayed healing in control groups. Hexosamine molecules form the ground substrate for extracellular matrix. The concentration of hexosamine was seen to be inversely proportional with progression of healing (Udhayakumar et al., 2017). A similar pattern of healing is reported by Mazlyzam et al. where the level of hexosamine was high on day 3 and decreased on day 6 when treated with the stem juice of *A. denudata* (AL et al., 2015). The presence of these glycosaminoglycans aid in stabilization of collagen fibers and facilitate cell adhesion and proliferation. The concentration of hexosamine on 4, 8, 12, and 16th day were monitored which is shown in **Fig. 7[f]**. However, the level of hexosamine was found to diminish gradually with the progress of wound healing and collagen deposition.

3. 2. 18. Assessment of regulatory cytokines

Fig. 9 indicates the immunohistochemical staining of MMP-2, MMP-9, TNFα post-burn wound days. The regulation of growth factors and the proteinase activity by MMP's play a dynamic role in the reconstruction of wound. So, in this study the expression of MMP during the course of healing was assessed (Shanmugasundaram et al., 2009). The level of MMP 2 and 9 was seen to be high in the samples taken on day 4 in all the groups. However, as the days progressed the expression of MMPs'diminished. In the non-infected group, MMP levels was reduced in day 8 while the infected groups showed higher levels of MMP because of the infection which hindered healing. A gradual decrease in the MMP expression was observed with the advancement of wound healing. The level of MMP 2 diminished from day 12 to undetectable levels from day 16 onwards which was also confirmed through gelatin zymography. As observed in the

immunohistochemical staining, the expression of MMP 2 seen in groups treated with Silvadene® and the nanoconstruct, induced cellular migration and thereby initiation of cell adhesion. The MMP-9 expressed in the same groups on day 8 aids in the re-epithelialization at the edges of the wound which is evidenced by the histochemical studies. Shanmugasundaram et al. had reported that the levels of MMP 2 was seen to be higher in the intial days after wounding while the expression of MMP 9 was profound as wound healing progressed. (Shanmugasundaram et al., 2009)

The immunohistochemical studies reveal the presence of the inflammatory cytokine (tumor necrosis factor α) indicating the preparatory process of wound healing. TNFα being an important inflammatory marker stimulates the adhesion and differentiation of fibroblasts. Its expression was observed in day 4 of group 3 and gradually reduced as wound healing progressed. Zhu et al. had reported that the expression of TNFα decreased in SA/GMs/Dex-HA hydrogel applied to full-thickness infected burn wound rat models (Zhu et al., 2018). When re-epithelialization begins, MMP's were observed which play a major role in degrading the ECM allowing vascularisation to begin. Thus, the presence of these cytokines signifies the induction of inflammation leading to angiogenesis upon treatment with the scaffold. **Fig. 9** indicates the immunohistochemical staining of MMP-2, MMP-9, TNFα in the burn wound treated with the scaffold (group 3)

4. Conclusion

In summary, the prospect of this study was designed perceiving the aspects of a burn patient with wound infection. Electrospinning of Poly-3-hydroxybutyric acid (P) and gelatin (G) yielded a nanofibrous matrix with excellent porosity, swelling index, offering the required degradability and mechanical strength. The highly porous morphology enabled oxygen transfer with conducive

environment for adhesion and proliferation of fibroblasts. The mechanical durability of the dressing reduces the strain of frequent dressing and hastens healing. The drug bound LDH, L-AgSD incorporated in the scaffold shielded the wound from infection at the tested concentration. *In-vivo* wound healing efficiency of the burn wounds were promising with the use of L-AgSD augmented nanofibrous construct. overall, the nanofibrous construct exhibited a positive influence on the process of wound healing in all perspectives.

Acknowledgement

The author Vimala Devi Mohan gratefully acknowledges financial support for this work through the grants awarded by the Department of Science and Technology (DST), New Delhi, India, (SR/WOS-A/ET-1060/2014). Financial support from ICMR (IRIS No.2013-1293.) and CSIR-CLRI under Translational Research Project OLP-09/TRP is acknowledged.

Author contributions

The manuscript was written through contributions of all authors. All authors have given approval to the final version of the manuscript.

Notes

The authors declare no competing financial interest.

Supplementary Information

Table S1 and detailed experimental methods section is given as supplementary information

References

Akhilesh K. Gaharwar, S.M., Karaca, E., Dolatshahi-Pirouz, A., Patel, A., Rangarajan, K., Silvia M. Mihaila, Iviglia, G., Zhang, H., Ali, K., 2014. Nanoclay-enriched poly(ε-caprolactone) electrospun scaffolds for osteogenic differentiation of human mesenchymal stem cells. TISSUE Eng. Part A 20, 2088–2101.

AL, M., Zaki, M.Z.M., Leng, T.M., Rahman, N.H.A., Arshad, S.A., Hamid, A., 2015. Alocasia denudata Engler treatment enhance open wound healing activities in Wistar rat's skin. J. Ethnopharmacol. 176, 258–267. https://doi.org/10.1016/j.jep.2015.10.036

Andreu, V., Mendoza, G., Arruebo, M., Irusta, S., 2015. Smart dressings based on nanostructured fibers containing natural origin antimicrobial, anti-inflammatory, and regenerative compounds. Materials (Basel). 8, 5154–5193. https://doi.org/10.3390/ma8085154

Arakha, M., Pal, S., Samantarrai, D., Panigrahi, T.K., Mallick, B.C., Pramanik, K., Mallick, B., Jha, S., 2015. Antimicrobial activity of iron oxide nanoparticle upon modulation of nanoparticle-bacteria interface. Sci. Rep. 5, 1–12. https://doi.org/10.1038/srep14813

Budyanto, L., Goh, Y.Q., Ooi, C.P., 2009. Fabrication of porous poly(L-lactide) (PLLA) scaffolds for tissue engineering using liquid-liquid phase separation and freeze extraction. J. Mater. Sci. Mater. Med. 20, 105–111. https://doi.org/10.1007/s10856-008-3545-8

Chakavala, S.R., Patel, N.G., Thakkar, V.T., Patel, K. V, Gandhi, T.R., 2012. Development and in vivo evaluation of silver sulfadiazine loaded hydrogel consisting polyvinyl alcohol and chitosan for severe burns. J Pharm Bioall Sci 4, 54–57. https://doi.org/10.4103/0975-7406.94131

Chakraborti, M., Jackson, J.K., Plackett, D., Gilchrist, S.E., Burt, H.M., 2012. The application of layered double hydroxide clay (LDH)-poly(lactide-co- glycolic acid) (PLGA) film composites for the controlled release of antibiotics. J. Mater. Sci. Mater. Med. 23, 1705–1713. https://doi.org/10.1007/s10856-012-4638-y

Chakraborty, J., Roychowdhury, S., Sengupta, S., Ghosh, S., 2013. Mg-Al layered double hydroxide-methotrexate nanohybrid drug delivery system: Evaluation of efficacy. Mater.

Sci. Eng. C 33, 2168–2174. https://doi.org/10.1016/j.msec.2013.01.047

Chandrasekaran, A.R., Venugopal, J., Sundarrajan, S., Ramakrishna, S., 2011. Fabrication of a nanofibrous scaffold with improved bioactivity for culture of human dermal fibroblasts for skin regeneration. Biomed. Mater. 6. https://doi.org/10.1088/1748-6041/6/1/015001

Chen, C., Cheng, Y.C., Yu, C.H., Chan, S.W., Cheung, M.K., Yu, P.H.F., 2008. In vitro cytotoxicity, hemolysis assay, and biodegradation behavior of biodegradable poly(3-hydroxybutyrate)-poly(ethylene glycol)-poly(3- hydroxybutyrate) nanoparticles as potential drug carriers. J. Biomed. Mater. Res. - Part A 87, 290–298. https://doi.org/10.1002/jbm.a.31719

Choi, H.M.C., Cheing, A.K.K., Ng, G.Y.F., Cheing, G.L.Y., 2018. Effects of pulsed electromagnetic field (PEMF) on the tensile biomechanical properties of diabetic wounds at different phases of healing 1–12.

Dai, M., Zheng, X., Xu, X., Kong, X., Li, X., Guo, G., Luo, F., Zhao, X., Wei, Y.Q., Qian, Z., 2009. Chitosan-Alginate Sponge : Preparation and Application in Curcumin Delivery for Dermal Wound Healing in Rat 2009. https://doi.org/10.1155/2009/595126

El-Feky, G.S., El-Banna, S.T., El-Bahy, G.S., Abdelrazek, E.M., Kamal, Em., 2017. Alginate coated chitosan nanogel for the controlled topical delivery of Silver sulfadiazine. Carbohydr. Polym. 177, 194–202. https://doi.org/10.1016/j.carbpol.2017.08.104

Elson, L.A., Morgan, and W.T.J., 1933. A COLORIMETRIC METHOD FOR THE DETERMINATION OF GLUCOSAMINE AND CHONDROSAMINE.

Fallah, M., Bahrami, S.H., Ranjbar-Mohammadi, M., 2016. Fabrication and characterization of PCL/gelatin/curcumin nanofibers and their antibacterial properties. J. Ind. Text. 46, 562–577. https://doi.org/10.1177/1528083715594978

596 Fang, L., Li, W., Chen, H., Xiao, F., Holm, P.E., Hansen, C.B., 2015. Synergistic effect of humic
597 and fulvic acids on Ni removal by the calcined Mg / Al 1–7.
598 Garg, T., Singh, O., Arora, S., Murthy, R.S.R., 2012. Scaffold: A Novel Carrier for Cell and
599 Drug Delivery. Crit. Rev. Ther. Drug Carr. Syst. 29, 1–63.
600 https://doi.org/10.1615/CritRevTherDrugCarrierSyst.v29.i1.10
601 Ge, N., Wang, D., Peng, F., Li, J., Qiao, Y., Liu, X., 2016. Poly(styrenesulfonate)-Modified Ni-
602 Ti Layered Double Hydroxide Film: A Smart Drug-Eluting Platform. ACS Appl. Mater.
603 Interfaces 8, 24491–24501. https://doi.org/10.1021/acsami.6b09697
604 Grzybowski, J., Janiak, M.K., Oidak, E., Lasocki, K., Wrembel-Wargocka, J., Cheda, A., Antos-
605 Bielska, M., Pojda, Z., 1999. New cytokine dressings. II. Stimulation of oxidative burst in
606 leucocytes in vitro and reduction of viable bacteria within an infected wound. Int. J. Pharm.
607 184, 179–187. https://doi.org/10.1016/S0378-5173(99)00064-2
608 Gu, Z., Thomas, A.C., Xu, Z.P., Campbell, J.H., Lu, G.Q., 2008. In vitro sustained release of
609 LMWH from MgAl-layered double hydroxide nanohybrids. Chem. Mater. 20, 3715–3722.
610 https://doi.org/10.1021/cm703602t
611 Heo, D.N., Yang, D.H., Lee, J.B., Bae, M.S., Kim, J.H., Moon, S.H., Chun, H.J., Kim, C.H.,
612 Lim, H.N., Kwon, I.K., 2013. Burn-wound healing effect of gelatin/polyurethane nanofiber
613 scaffold containing silver-sulfadiazine. J. Biomed. Nanotechnol. 9, 511–515.
614 https://doi.org/10.1166/jbn.2013.1509
615 J. Woessner, J., 1961. The Determination of Hydroxyproline in Tisuue and Protein Samples
616 Containing Small Proportions of this Imino Acid. Arch. Biochem. Biophys. 93, 440–447.
617 Jahromi, M.A.M., Zangabad, P.S., Basri, S.M.M., Zangabad, K.S., Ghamarypour, A., Aref, A.R.,
618 Karimi, M., Hamblin, M.R., 2018. Nanomedicine and advanced technologies for burns:

Preventing infection and facilitating wound healing. Adv. Drug Deliv. Rev. 123, 33–64. https://doi.org/10.1016/j.addr.2017.08.001

Jiang, J., Carlson, M.A., Teusink, M.J., Wang, H., MacEwan, M.R., Xie, J., 2015. Expanding Two-Dimensional Electrospun Nanofiber Membranes in the Third Dimension by a Modified Gas-Foaming Technique. ACS Biomater. Sci. Eng. 1, 991–1001. https://doi.org/10.1021/acsbiomaterials.5b00238

Jin, L., Liu, Q., Sun, Z., Ni, X., Wei, M., 2010. Preparation of 5-fluorouracil/β-cyclodextrin complex intercalated in layered double hydroxide and the controlled drug release properties. Ind. Eng. Chem. Res. 49, 11176–11181. https://doi.org/10.1021/ie100990z

Jithendra, P., Rajam, A.M., Kalaivani, T., Mandal, A.B., Rose, C., 2013. Preparation and characterization of aloe vera blended Collagen-Chitosan composite scaffold for tissue engineering applications. ACS Appl. Mater. Interfaces 5, 7291–7298. https://doi.org/10.1021/am401637c

Kim, S.E., Wang, J., Jordan, A.M., Korley, L.T.J., Baer, E., Pokorski, J.K., 2014. Surface modification of melt extruded poly(μ-caprolactone) nanofibers: Toward a new scalable biomaterial scaffold. ACS Macro Lett. 3, 585–589. https://doi.org/10.1021/mz500112d

Klemkaite, K., Prosycevas, I., Taraskevicius, R., Khinsky, A., Kareiva, A., 2011. Synthesis and characterization of layered double hydroxides with different cations (Mg, Co, Ni, Al), decomposition and reformation of mixed metal oxides to layered structures. Cent. Eur. J. Chem. 9, 275–282. https://doi.org/10.2478/s11532-011-0007-9

Li, M., Ogiso, M., Minoura, N., 2003. Enzymatic degradation behavior of porous silk fibroin sheets. Biomaterials 24, 357–365. https://doi.org/10.1016/S0142-9612(02)00326-5

Li, P., Xu, X., Wu, L., Li, B., Zhao, Y., 2015. Synthesis of silver nanoparticles loaded

642 sulfadiazine/polyvinyl alcohol nanorods and their antibacterial activities. Med. Chem.
643 Commun. 6, 2204–2208. https://doi.org/10.1039/C5MD00331H
644 Liji, L.S., Mehedi, R., Malmivirta, M., Paturi, P., Lastusaari, M., Dîrtu, M.M., Garcia, Y.,
645 Fardim, P., 2016. Heteronuclear nanoparticles supported hydrotalcites containing Ni(II) and
646 Fe(III) stable photocatalysts for Orange II degradation. Appl. Clay Sci. 132–133, 641–649.
647 https://doi.org/10.1016/j.clay.2016.08.016
648 Lin, J., Li, C., Zhao, Y., Hu, J., Zhang, L.M., 2012. Co-electrospun nanofibrous membranes of
649 collagen and zein for wound healing. ACS Appl. Mater. Interfaces 4, 1050–1057.
650 https://doi.org/10.1021/am201669z
651 Liu, J., Lu, F., Chen, H., Bao, R., Li, Z., Lu, B., Yu, K., Dai, F., Wu, D., Lan, G., 2017. Healing
652 of skin wounds using a new cocoon scaffold loaded with platelet-rich or platelet-poor
653 plasma. RSC Adv. 7, 6474–6485. https://doi.org/10.1039/C6RA27021B
654 Manikandan, A., Mani, M.P., Jaganathan, S.K., Rajasekar, R., Jagannath, M., 2017. Formation of
655 functional nanofibrous electrospun polyurethane and murivenna oil with improved
656 haemocompatibility for wound healing. Polym. Test. 61, 106–113.
657 https://doi.org/10.1016/j.polymertesting.2017.05.008
658 Martin, C., Low, W.L., Amin, M.C.I.M., Radecka, I., Raj, P., Kenward, K., 2013. Current trends
659 in the development of wound dressings, biomaterials and devices. Pharm. Pat. Anal. 2, 341–
660 359. https://doi.org/10.4155/ppa.13.18
661 Martín, J., Maiz, J., Sacristan, J., Mijangos, C., 2012. Tailored polymer-based nanorods and
662 nanotubes by “template synthesis”: From preparation to applications. Polymer (Guildf). 53,
663 1149–1166. https://doi.org/10.1016/j.polymer.2012.01.028
664 Muthukumar, T., Prabu, P., Ghosh, K., Sastry, T.P., 2014. Fish scale collagen sponge

665 incorporated with Macrotyloma uniflorum plant extract as a possible wound/burn dressing
666 material. Colloids Surfaces B Biointerfaces 113, 207–212.
667 https://doi.org/10.1016/j.colsurfb.2013.09.019
668 Nagiah, N., Madhavi, L., Anitha, R., Anandan, C., Srinivasan, N.T., Sivagnanam, U.T., 2013a.
669 Development and characterization of coaxially electrospun gelatin coated poly (3-
670 hydroxybutyric acid) thin films as potential scaffolds for skin regeneration. Mater. Sci. Eng.
671 C 33, 4444–4452. https://doi.org/10.1016/j.msec.2013.06.042
672 Nagiah, N., Madhavi, L., Anitha, R., Srinivasan, N.T., Sivagnanam, U.T., 2013b.
673 Electrospinning of poly (3-hydroxybutyric acid) and gelatin blended thin films: Fabrication,
674 characterization, and application in skin regeneration. Polym. Bull. 70, 2337–2358.
675 https://doi.org/10.1007/s00289-013-0956-6
676 O'Brien, F.J., 2011. Biomaterials & scaffolds for tissue engineering. Mater. Today 14, 88–95.
677 https://doi.org/10.1016/S1369-7021(11)70058-X
678 Ouyang, Q., Hu, Z., Lin, Z., Quan, W., Deng, Y., Li, S., Li, P., Chen, Y., 2018. International
679 Journal of Biological Macromolecules Chitosan hydrogel in combination with marine
680 peptides from tilapia for burns healing. Int. J. Biol. Macromol. 112, 1191–1198.
681 https://doi.org/10.1016/j.ijbiomac.2018.01.217
682 Pan, D., Zhang, H., Zhang, T., Duan, X., 2010. A novel organic-inorganic microhybrids
683 containing anticancer agent doxifluridine and layered double hydroxides: Structure and
684 controlled release properties. Chem. Eng. Sci. 65, 3762–3771.
685 https://doi.org/10.1016/j.ces.2010.03.013
686 Parvinzadeh, M., Moradian, S., Rashidi, A., Yazdanshenas, M.E., 2010. Effect of the addition of
687 modified nanoclays on the surface properties of the resultant polyethylene terephthalate/clay

nanocomposites. Polym. - Plast. Technol. Eng. 49, 874–884. https://doi.org/10.1080/03602551003664628

Qing Qin, Ya Liu, Si-Chong Chen, Fei-Yu Zhai, Xin-Ke Jing, Y.Z.W., 2012. Electrospinning Fabrication and Characterization of Poly(vinyl alcohol)/Layered Double Hydroxides Composite Fibers. J. Polym. Appl. Sci. 126. https://doi.org/10.1002/app.36876

Qiu, D. peng, Hou, W. guo, 2009. Synthesis and characterization of indole-3-butyric acid/hydrotalcite-like compound nanohybrids. Colloids Surfaces A Physicochem. Eng. Asp. 336, 12–17. https://doi.org/10.1016/j.colsurfa.2008.11.028

Ramanathan, G., Singaravelu, S., Raja, M.D., Nagiah, N., Padmapriya, P., Ruban, K., Kaveri, K., Natarajan, T.S., Sivagnanam, U.T., Perumal, P.T., 2016. Fabrication and characterization of a collagen coated electrospun poly(3-hydroxybutyric acid)-gelatin nanofibrous scaffold as a soft bio-mimetic material for skin tissue engineering applications. RSC Adv. 6, 7914–7922. https://doi.org/10.1039/c5ra19529b

Rathore, H.S., Sarubala, M., Ramanathan, G., Singaravelu, S., Raja, M.D., Gupta, S., Sivagnanam, U.T., 2016. Fabrication of biomimetic porous novel sponge from gum kondagogu for wound dressing. Mater. Lett. 177, 108–111. https://doi.org/10.1016/j.matlet.2016.04.185

Sano, S., Fujimori, R., Takashima, M., Itokawa, Y., 1982. Absorption, excretion and tissue distribution of silver sulfadiazine. Burns 8, 278–285. https://doi.org/10.1016/0305-4179(82)90010-9

Shafiei, S.S., Shavandi, M., Ahangari, G., Shokrolahi, F., 2016. Electrospun layered double hydroxide/poly (ε-caprolactone) nanocomposite scaffolds for adipogenic differentiation of adipose-derived mesenchymal stem cells. Appl. Clay Sci. 127–128, 52–63.

https://doi.org/10.1016/j.clay.2016.04.004

Shafiei, S.S., Solati-Hashjin, M., Samadikuchaksaraei, A., Kalantarinejad, R., Asadi-Eydivand, M., Abu Osman, N.A., 2015. Epigallocatechin gallate/layered double hydroxide nanohybrids: Preparation, characterization, and in vitro anti-tumor study. PLoS One 10, 1–18. https://doi.org/10.1371/journal.pone.0136530

Shanmugasundaram, N., Uma, T.S., Lakshmi, T.S.R., Babu, M., 2009. Efficiency of controlled topical delivery of silver sulfadiazine in infected burn wounds. J. Biomed. Mater. Res. - Part A 89, 472–482. https://doi.org/10.1002/jbm.a.31997

Shao, W., Wu, J., Wang, S., Huang, M., Liu, X., Zhang, R., 2017. Construction of silver sulfadiazine loaded chitosan composite sponges as potential wound dressings. Carbohydr. Polym. 157, 1963–1970. https://doi.org/10.1016/j.carbpol.2016.11.087

Singaravelu, S., Ramanathan, G., Sivagnanam, U.T., 2017. Dual-layered 3D nanofibrous matrix incorporated with dual drugs and their synergetic effect on accelerating wound healing through growth factor regulation. Mater. Sci. Eng. C 76, 37–49. https://doi.org/10.1016/j.msec.2017.02.148

Smith, L.A., Ma, P.X., 2004. Nano-fibrous scaffolds for tissue engineering. Colloids Surfaces B Biointerfaces 39, 125–131. https://doi.org/10.1016/j.colsurfb.2003.12.004

Sobhana, L., Sarakha, M., Prevot, V., Fardim, P., 2016. Layered double hydroxides decorated with Au-Pd nanoparticles to photodegradate Orange II from water. Appl. Clay Sci. 134, 120–127. https://doi.org/10.1016/j.clay.2016.06.019

Sobhana, S.S.L., Bogati, D.R., Reza, M., Gustafsson, J., Fardim, P., 2016. Cellulose biotemplates for layered double hydroxides networks. Microporous Mesoporous Mater. 225, 66–73. https://doi.org/10.1016/j.micromeso.2015.12.009

734 Sobhana, S.S.L., Zhang, X., Kesavan, L., Liias, P., Fardim, P., 2017. Layered double hydroxide
735 interfaced stearic acid – Cellulose fibres: A new class of super-hydrophobic hybrid
736 materials. Colloids Surfaces A Physicochem. Eng. Asp. 522, 416–424.
737 https://doi.org/10.1016/j.colsurfa.2017.03.025
738 Taepaiboon, P., Rungsardthong, U., Supaphol, P., 2006. Drug-loaded electrospun mats of
739 poly(vinyl alcohol) fibres and their release characteristics of four model drugs.
740 Nanotechnology 17, 2317–2329. https://doi.org/10.1088/0957-4484/17/9/041
741 Timmers, M.S., Graafland, N., Bernards, A.T., Nelissen, R.G.H.H., Dissel, J.T. Van, Jukema,
742 G.N., 2008. Negative pressure wound treatment with polyvinyl alcohol foam and
743 polyhexanide antiseptic solution instillation in posttraumatic osteomyelitis.
744 https://doi.org/10.1111/j.1524-475X.2009.00458.x
745 Udhayakumar, S., Shankar, K.G., Sowndarya, S., 2017. RSC Advances engineering and
746 regeneration : in silico , in vitro , and. RSC Adv. 7, 25070–25088.
747 https://doi.org/10.1039/C7RA02842C
748 Unnithan, A.R., Barakat, N.A.M., Tirupathi Pichiah, P.B., Gnanasekaran, G., Nirmala, R., Cha,
749 Y.S., Jung, C.H., El-Newehy, M., Kim, H.Y., 2012. Wound-dressing materials with
750 antibacterial activity from electrospun polyurethane-dextran nanofiber mats containing
751 ciprofloxacin HCl. Carbohydr. Polym. 90, 1786–1793.
752 https://doi.org/10.1016/j.carbpol.2012.07.071
753 Valarezo, E., Tammaro, L., González, S., Malagón, O., Vittoria, V., 2013b. Fabrication and
754 sustained release properties of poly(ε-caprolactone) electrospun fibers loaded with layered
755 double hydroxide nanoparticles intercalated with amoxicillin. Appl. Clay Sci. 72, 104–109.
756 https://doi.org/10.1016/j.clay.2012.12.006

Vatankhah, E., Prabhakaran, M.P., Semnani, D., Razavi, S., Morshed, M., Ramakrishna, S., 2014. Electrospun tecophilic/gelatin nanofibers with potential for small diameter blood vessel tissue engineering. Biopolymers 101, 1165–1180. https://doi.org/10.1002/bip.22524

Williams, G.R., Dunbar, T.G., Beer, A.J., Fogg, A.M., O'Hare, D., 2006. Intercalation chemistry of the novel layered double hydroxides MAl4(OH)(12) (NO3)(2)center dot gamma H2O (M = Zn, Cu, Ni and Co). 1: New organic intercalates and reaction mechanisms. J. Mater. Chem. 16, 1222–1230. https://doi.org/10.1039/b514874j

Xing, Z.C., Chae, W.P., Baek, J.Y., Choi, M.J., Jung, Y., Kang, I.K., 2010. In vitro assessment of antibacterial activity and cytocompatibility of silver-containing phbv nanofibrous scaffolds for tissue engineering. Biomacromolecules 11, 1248–1253. https://doi.org/10.1021/bm1000372

Xu, Z., Shi, L., Yang, M., Zhang, H., Zhu, L., 2015. Fabrication of a novel blended membrane with chitosan and silk microfibers for wound healing: characterization, in vitro and in vivo studies. J. Mater. Chem. B 3, 3634–3642. https://doi.org/10.1039/C5TB00226E

Zepon, K.M., Petronilho, F., Soldi, V., Salmoria, G.V., Kanis, L.A., 2014. Production and characterization of cornstarch/cellulose acetate/silver sulfadiazine extrudate matrices. Mater. Sci. Eng. C 44, 225–233. https://doi.org/10.1016/j.msec.2014.08.011

Zhong, S.P., Teo, W.E., Zhu, X., Beuerman, R., Ramakrishna, S., Yung, L.Y.L., 2007. Development of a novel collagen-GAG nanofibrous scaffold via electrospinning. Mater. Sci. Eng. C 27, 262–266. https://doi.org/10.1016/j.msec.2006.05.010

Zhu, Q., A, Jiang, M., A, Liu, Q., B, Yan, S., A, Feng, L., A, Lan, Y., C, Shan, G., D, Xue, W.G., 2018. Enhanced Healing Activity of Burn Wound Infection by Dextran-HA Hydrogel Enriched with Sanguinarine. Biomater. Sci. 6, 2472–2486.

https://doi.org/10.1039/C8BM00478A

Zou, F., Sun, X., Wang, X., 2019. Elastic, hydrophilic and biodegradable poly (1, 8-octanediol-co-citric acid)/polylactic acid nanofibrous membranes for potential wound dressing applications. Polym. Degrad. Stab. 166, 163–173.

Table captions

Table 1 Mechanical properties of electrospun nanofibrous matrices

Figure Captions

Figure 1 [a] Creation of burn wound with a temperature-controlled soldering rod, [b] Structure of silver sulfadazine (AgSD), [c] X-ray diffractogram of as-synthesized LDH, AgSD and L-AgSD. * denotes AgSD reflections and # denotes LDH reflections, [d] FTIR spectrum of as-synthesized LDH, AgSD and L-AgSD. * denotes AgSD reflections and # denotes LDH reflections, [e] TGA profiles of as-synthesized LDH and L-AgSD, [f] Particle size distribution of as-synthesized LDH and L-AgSD

Figure 2 [a & b] SEM, [c & d] elemental mapping images of MgAl LDH and L-AgSD respectively, [e] X-ray diffractogram of nanofibrous matrix containing (A) GP, (B) GP-AgSD, (C) GP-L, (D) GP-$(L\text{-}AgSD)_5$, (E) GP-$(L\text{-}AgSD)_{25}$ and (F) GP-$(L\text{-}AgSD)_{50}$ and [d] Thermo gravimetric curves of nanofibrous matrix

Figure 3 [a & b] HRSEM micrographs and [c & d] elemental mapping images of GP and GP-$(L\text{-}AgSD)_{25}$ nanofibrous matrix respectively. Inset shows the digital photograph of GP-$(L\text{-}AgSD)_{25}$, Atomic force micrograph of nanofibrous matrix containing [A] GP, [B] GP-$(L\text{-}AgSD)_5$, [C] GP-$(L\text{-}AgSD)_{25}$ and [D] GP-$(L\text{-}AgSD)_{50}$

Figure 4 [a] Porosity measurements of the nanofibrous matrix, [b] Water contact angle of various electrospun nanofibrous matrix, [c] Swelling behavior of the nanofibrous matrix, [d] *In*

vitro degradation of the nanofibrous matrix using collagenase enzyme, [e] *In vitro* drug release profiles of AgSD from electrospun nanofibrous matrix, [f] *In vitro* release profile of AgSD from matrix containing GP-$AgSD_{25}$ and GP-$(L\text{-}AgSD)_{25,}$ Fluorescence microscopy images of *Pseudomonas aeruginosa* (A) untreated and (B) treated with GP-$(L\text{-}AgSD)_{25}$ followed by staining with SYTO 9 and PI. The images were recorded at 40× magnification using a fluorescence microscope

Figure 5 [a] Digital photographs of red blood cells exposed to electrospun nanofibrous matrix. PC: Positive control; NC: Negative control; (A) GP, (B) GP-$(L\text{-}AgSD)_5$, (C) GP-$(L\text{-}AgSD)_{25}$ and (D) GP-$(L\text{-}AgSD)_{50}$, [b] Hemolytic activity of electrospun nanofibrous matrix, [c] *In vitro* biocompatibility of NIH 3T3 fibroblasts cells on 6, 24, 72 and 168 h using MTT assay, [d] Calcein AM-DAPI fluorescence staining images of NIH 3T3 fibroblasts' cell adherence and proliferation onto GP-$(L\text{-}AgSD)_{25}$ nanofibrous matrix at 6, 24, 72 and 168 h. The scale bar is 75 µm

Figure 6 Optical photographs depicting the progress of wound healing till 20 days

Figure 7 [a] Quantitative wound closure rate of control and treated groups, [b] Comparison of variations in body weight of control and treated groups. $*P< 0.05$ compared between day 0, 4, 8 and 12 of group 1 and 2; day 0, 4, 8, 12 and 16 of group 3 and 4; $*P< 0.05$ compared between day 0 and 12 of group 6; # $P< 0.01$ compared between day 0 and day 16 of group 5; day 0 and 4 of group 7. [c] Tensile strength of healed wound tissues of control and treated groups. $*P< 0.05$ compared with group 7; $**P< 0.01$ compared with group 7; $***$ $P< 0.001$ compared with group 7; # $P< 0.05$ compared with group 2. [d] Elongation at break of healed wound tissues of control and treated groups. $*$ $P< 0.05$ compared between group 1 and 7, 2 and 3, 3 and 6;♦ $P< 0.01$ compared with group 7; # $P< 0.001$ compared with group 7. [e] Effect of the nanofibrous matrix

on the hydroxyproline content. ∗P< 0.01 compared with day 4 and 12 in group 1, to 6 except group 2; ∗P< 0.01 compared with day 4 and 16 in group 1, 2 and 6; ∗P< 0.01 compared with day 8 and 12 in group 3; ∗P< 0.01 compared with day 8 and 16 in group 1and 7. [f] Effect of the nanofibrous matrix on the hexosamine content. ∗P< 0.05 compared with day 4 and day 12 in the non-infected group; ∗P< 0.05 compared with day 4 and day 12 in the Silvadene® treated group

Figure 8 H&E images of control and treated groups on 4^{th} (A, C, E, G) and 16^{th} day (B, D, F, H) post wounding; MT images of control and treated groups on 4^{th} (I, K, M, O) and 16^{th} day (J, L, N, P) post wounding (magnification: 40×). Group 1: Non-infected control, group 2: Infected control, group 3: GP-(L-AgSD), group 7: Silvadene®. N, C, E, WM and HF refers to the neutrophils, collagen, epidermis, wound margin and hair follicle respectively. The scale bar is 100 µm

Figure 9 Immunohistochemical staining for MMP 2, MMP9 and TNFα post-burn days. The scale bar is 340 µm

Graphical Abstract

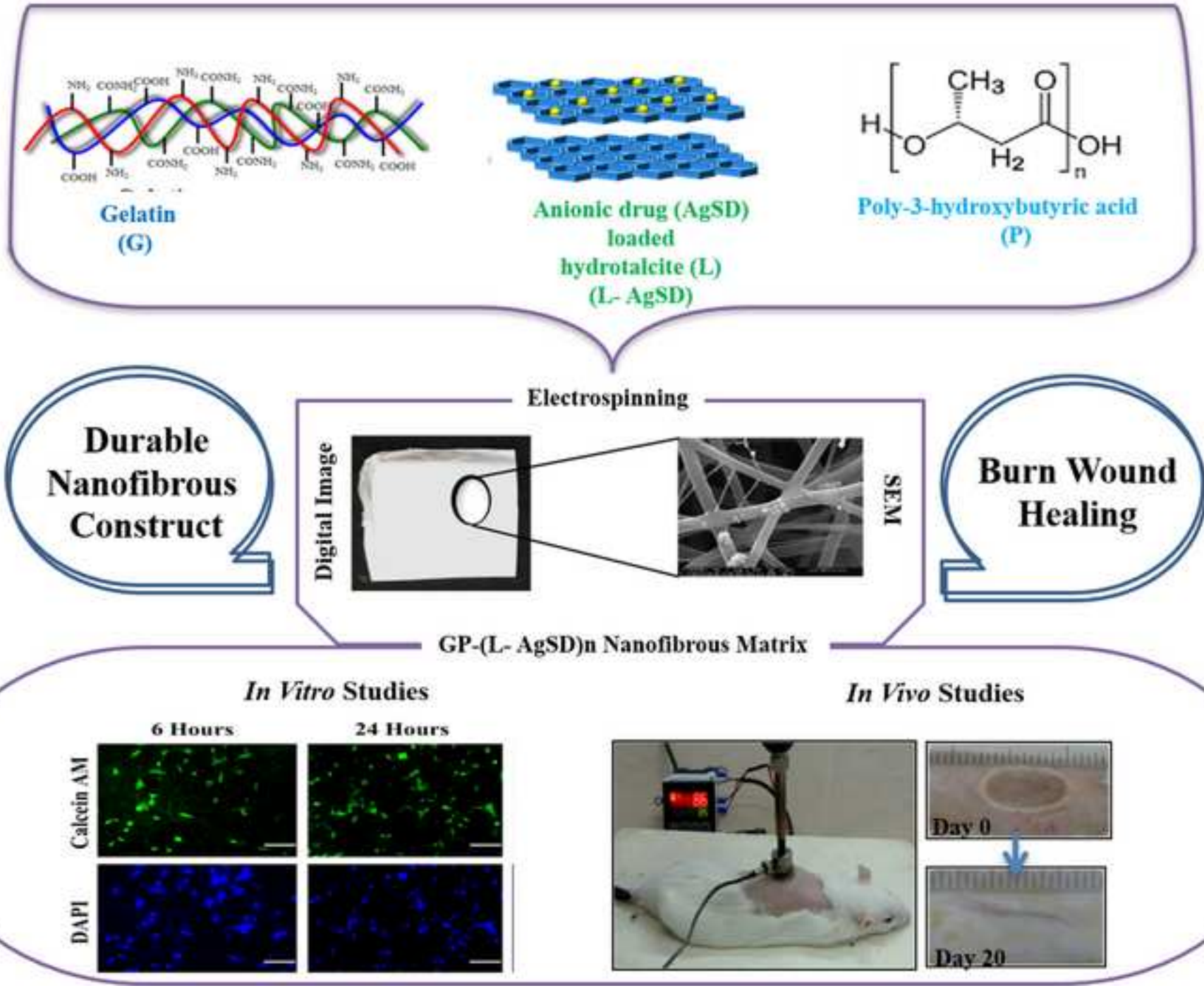

Highlights:

- Anionic drug (AgSD) with hydrotalcite (L) (L-AgSD) as a durable nanofibrous construct
- GP-$(L\text{-}AgSD)_n$ was fabricated as a nanofibrous hybrid construct with hydrotalcite
- Scaffolds exhibited desirable porosity, tensile strength, and swelling behavior
- Drug release behavior and antibacterial action was excellent with GP-$(L\text{-}AgSD)_n$ matrix
- Nanofibrous construct were biocompatible, promoted cell adhesion and proliferation
- Healing efficiency of the burn wounds were promising with GP-$(L\text{-}AgSD)_n$ matrix

Table 1: Mechanical properties of electrospun nanofibrous matrices

Samples	Mean tensile strength (MPa)	Mean elongation at break (%)
GP	3.12 ± 0.10	3.72 ± 0.13
GP-(L-AgSD)$_5$	4.21 ± 0.24	2.67 ± 0.09
GP-(L-AgSD)$_{25}$	5.32 ± 0.14	3.57 ± 0.26
GP-(L-AgSD)$_{50}$	7.88 ± 0.12	3.44 ± 0.11

Figure 3

Click here to download high resolution image

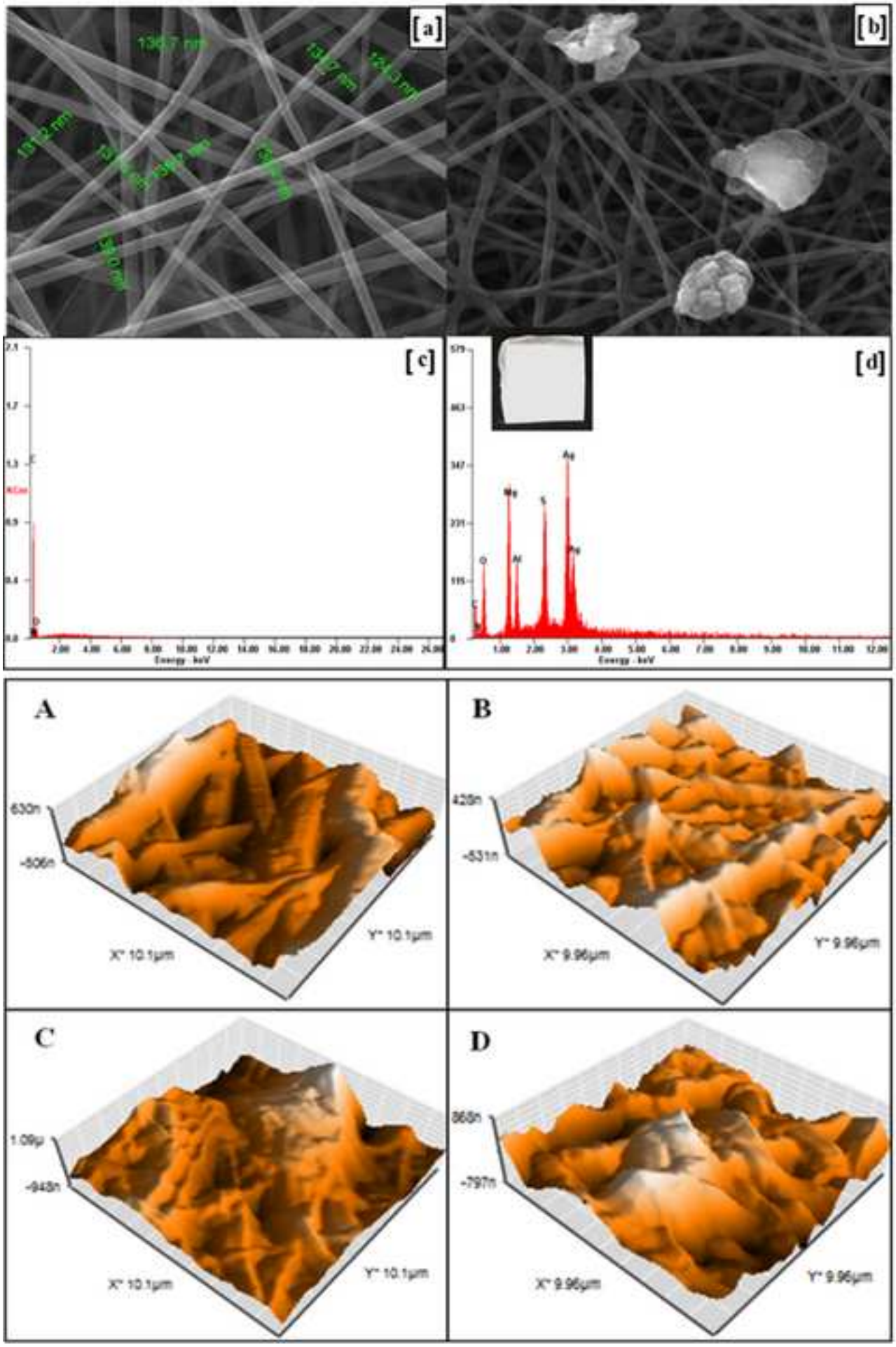

Figure 4

Click here to download high resolution image

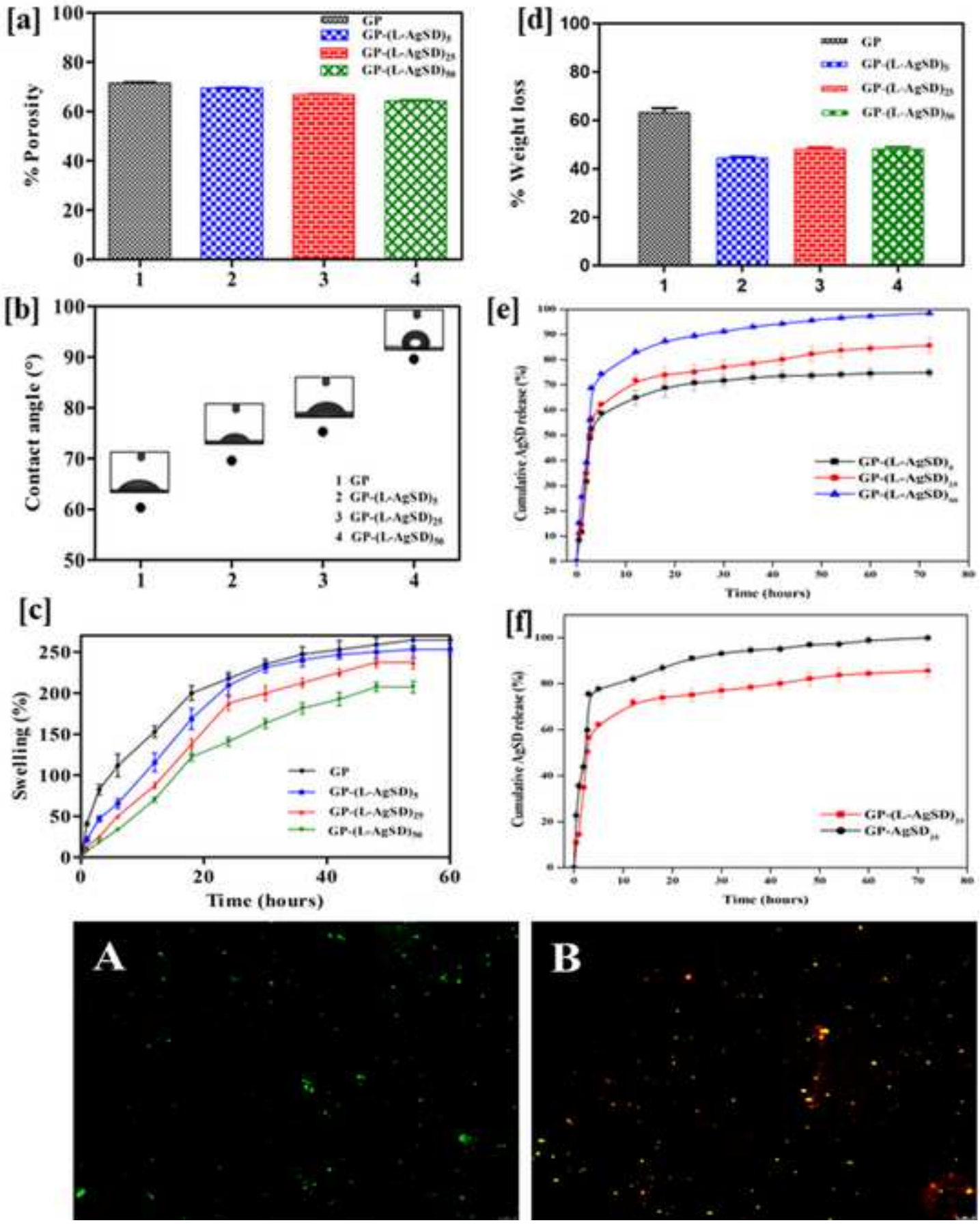

Figure 5

Click here to download high resolution image

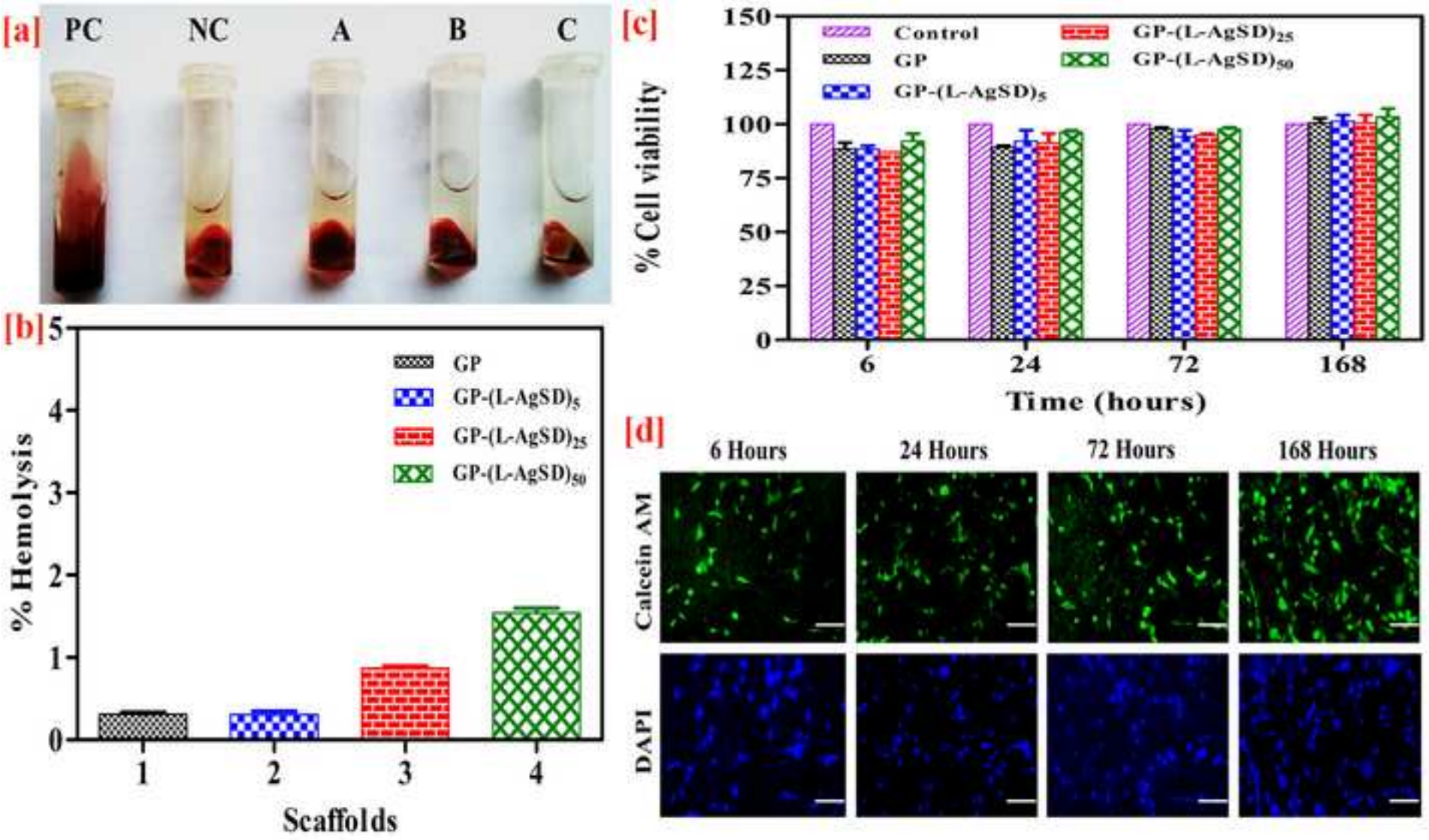

Figure 6

Click here to download high resolution image

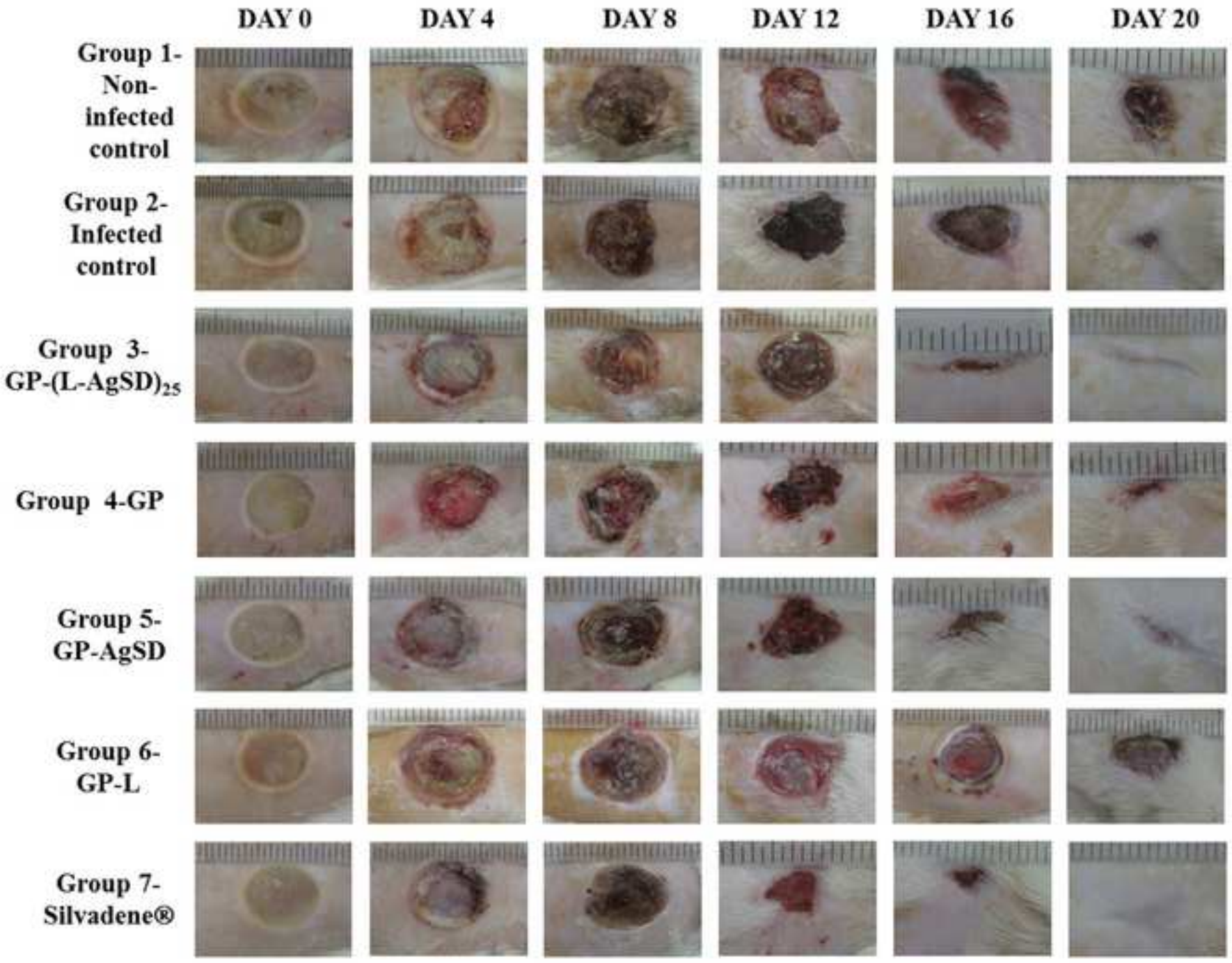

Figure 7

Click here to download high resolution image

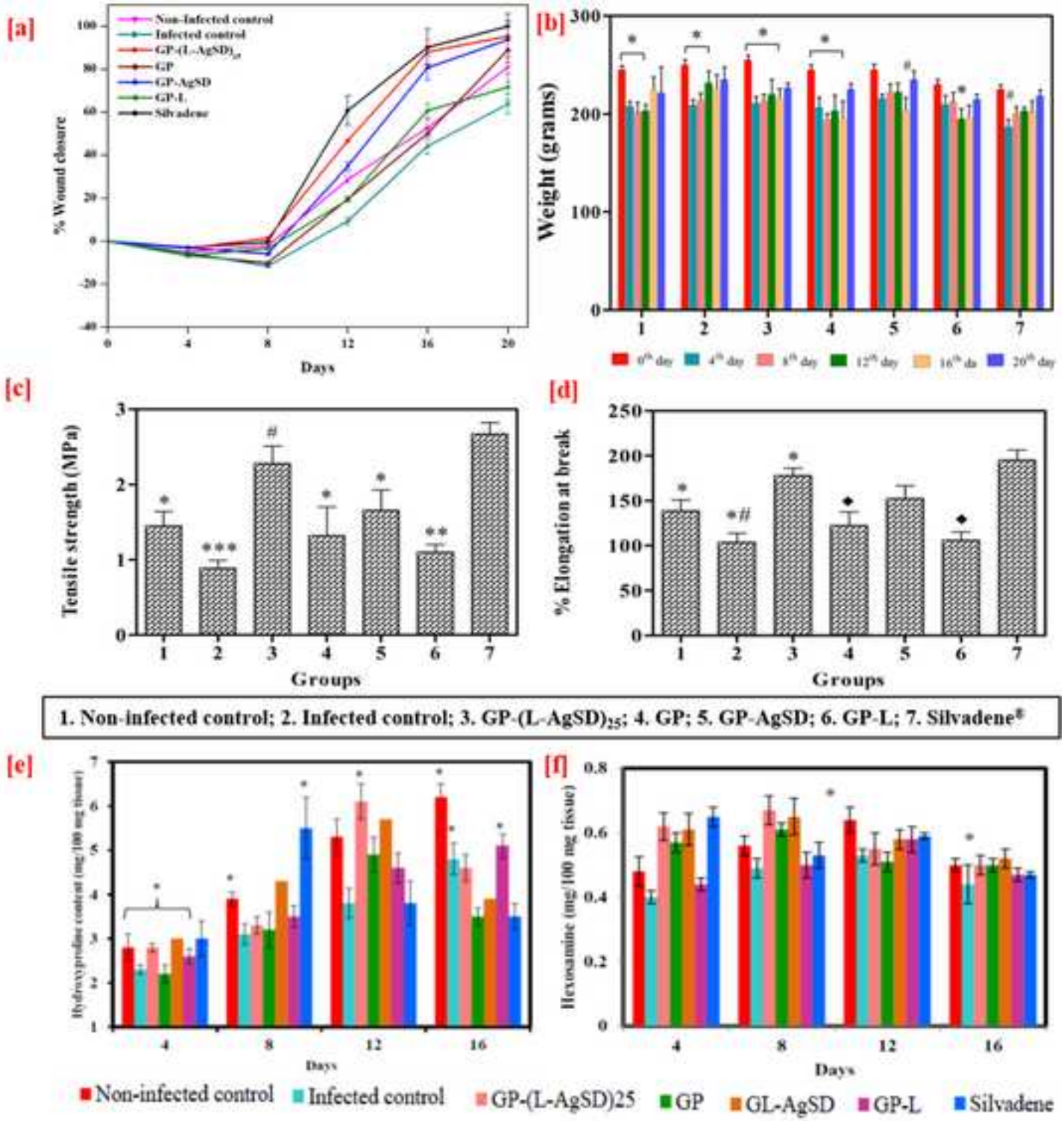

Figure 9

Click here to download high resolution image

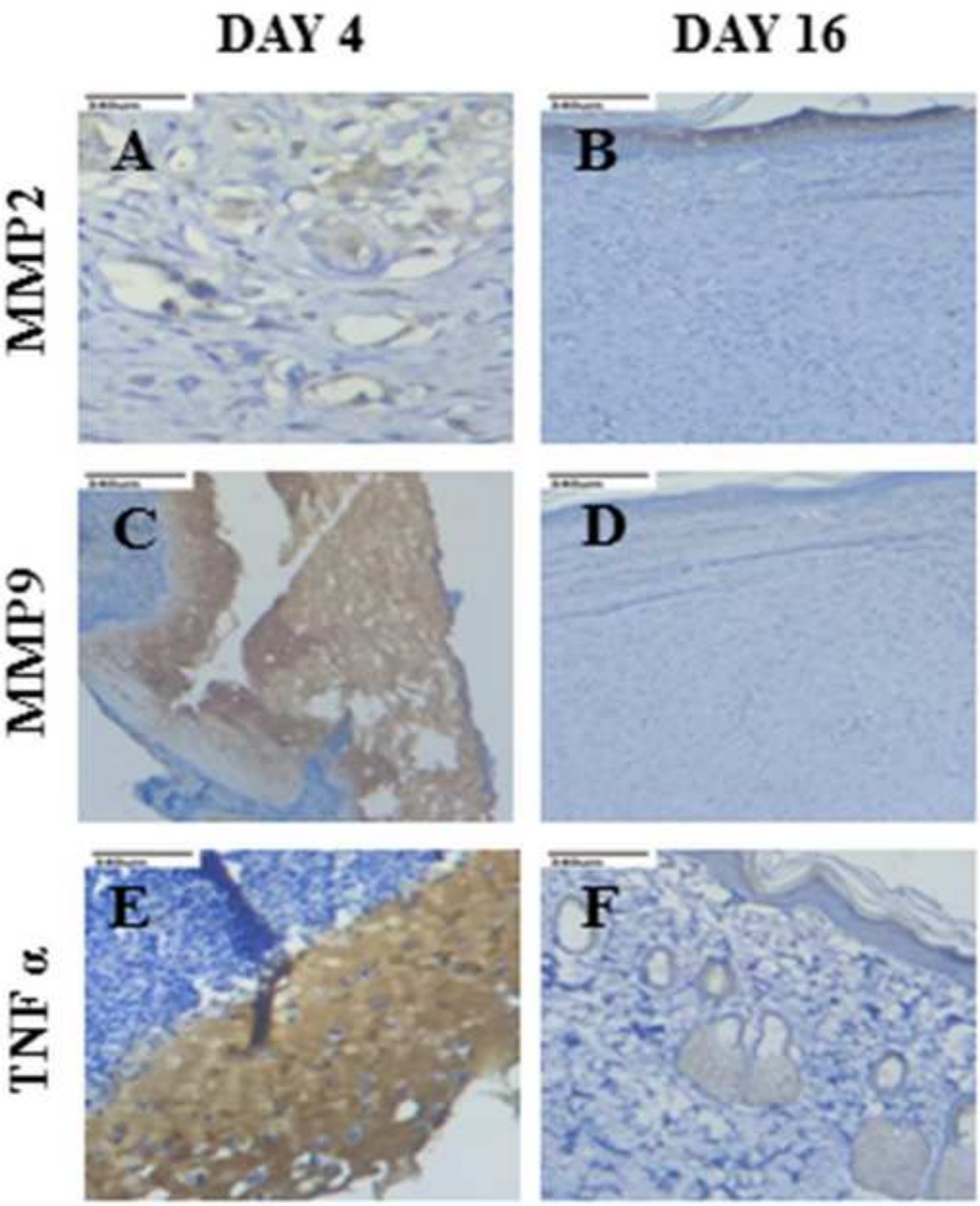

Figure 1

Click here to download high resolution image

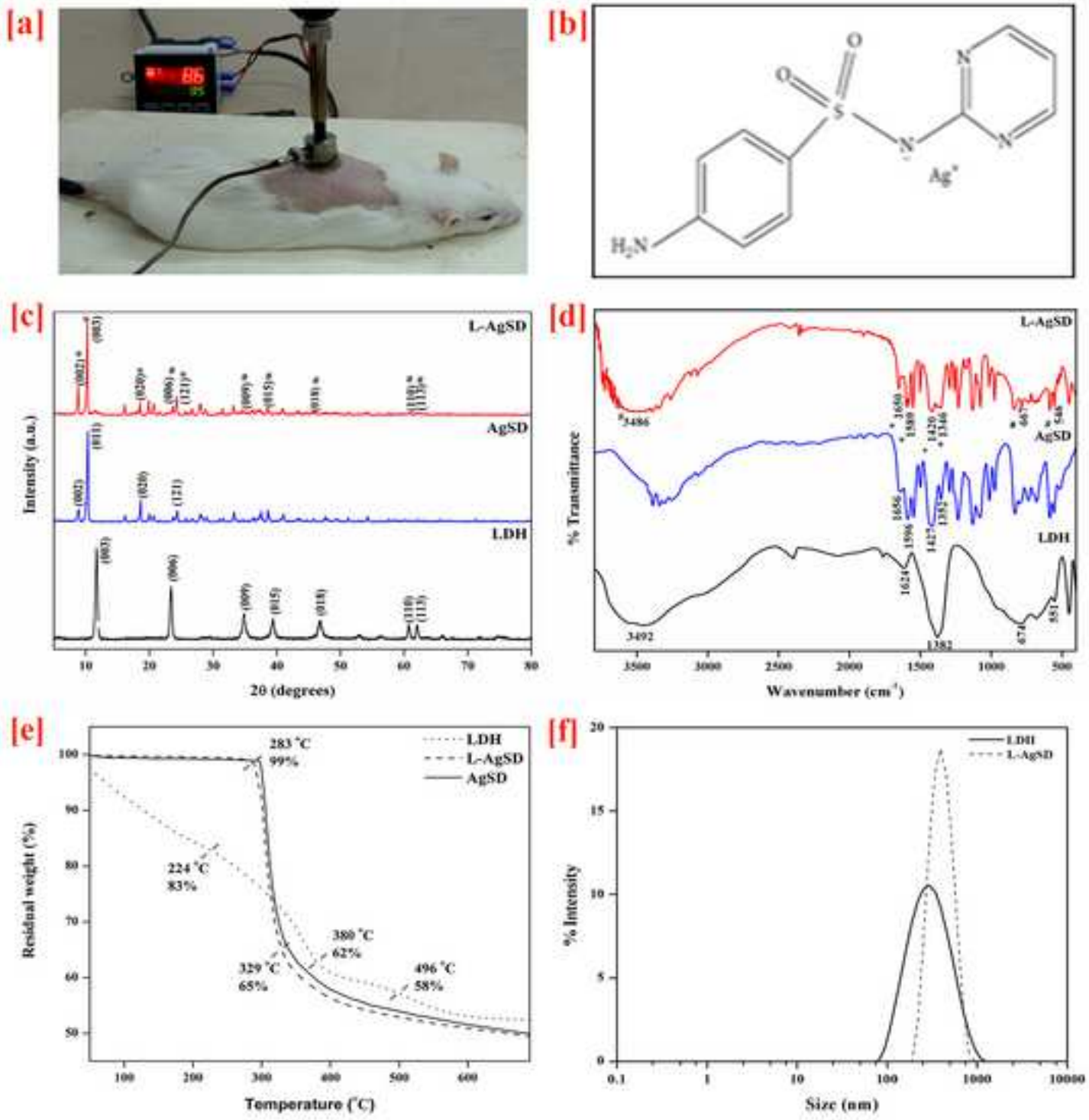

Figure 2

Click here to download high resolution image

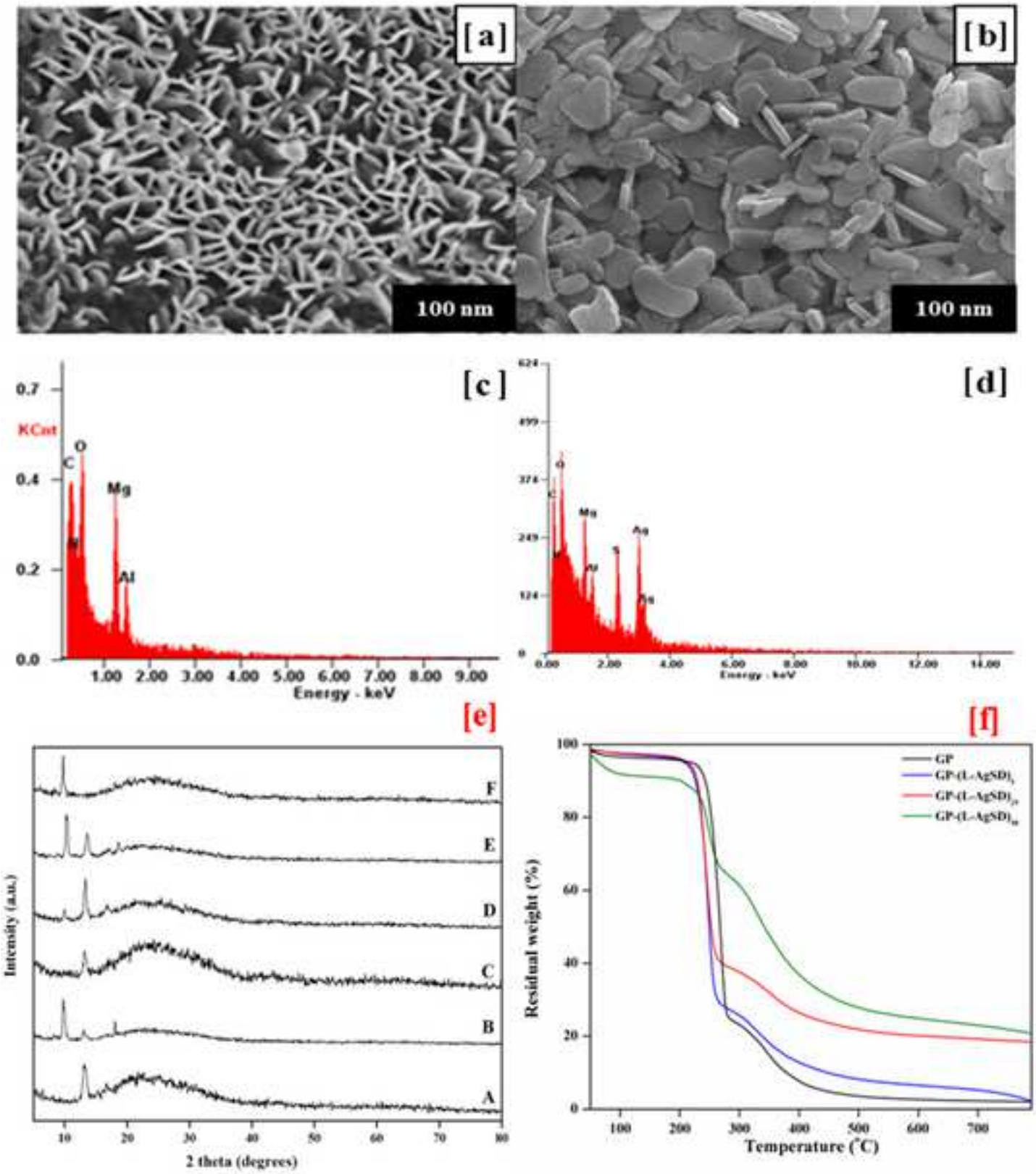

Figure 8

Click here to download high resolution image

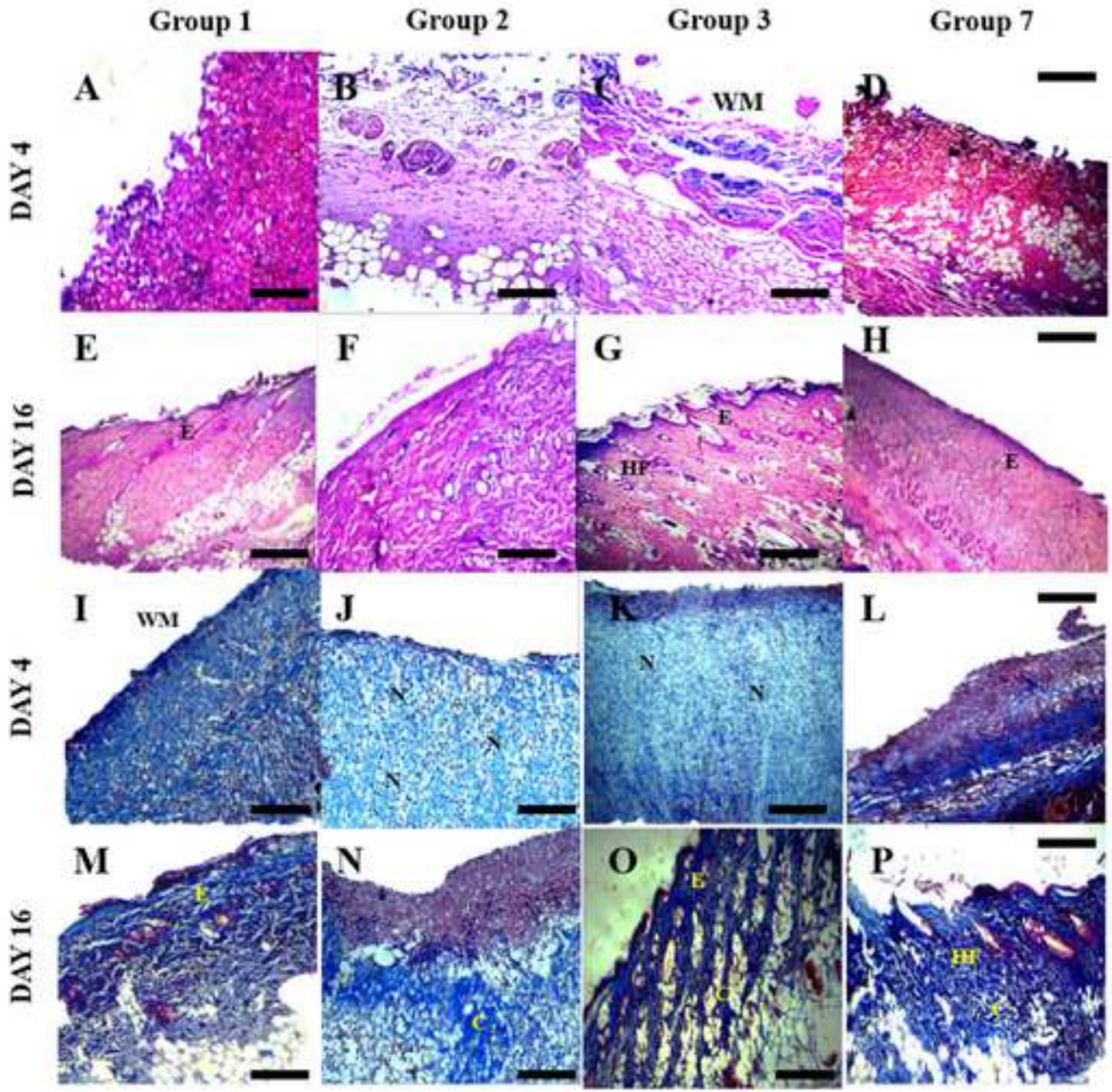

Abstract

Electrospinning of Gelatin (G) and Poly-3-hydroxybutyric acid (P) incorporated with anionic drug (AgSD) loaded hydrotalcite (L) (L-AgSD) is carried out to fabricate a nanofibrous scaffold which would recreate the native extracellular matrix suitable for cutaneous regeneration. The L-AgSD complex was augmented into electrospun nanofibers of diameter 100-140 nm. The physiochemical (XRD, FTIR), morphological (SEM), mechanical (tensile strength) and biological (*in vitro* and *in vivo*) properties of the developed wound construct were studied. Antimicrobial studies reveal the potential activity against microbial infection. Studies on drug release kinetics demonstrate a controlled drug release of 86% in 72 hours. *In vitro* biocompatibility studies using NIH 3T3 fibroblast cell line showed excellent cell adhesion and cell proliferation indicating the biocompatible nature of the scaffold. The matrix accelerated wound healing on *Pseudomonas* infected burn wound induced on rat models. The tailored matrix is promising as an impending nanohybrid construct for burn wound injuries with controlled drug release and antibacterial activity.

Keywords: Burns; Wound Healing; Nanofibrous matrix; LDH; Biocompatibility; *In vivo* study.

Background dataset for online publication only

Click here to download Background dataset for online publication only: R2 Revised supplementary information - no changes ma

*Declaration of Interest Statement

Declaration of interests

☒ The authors declare that they have no known competing financial interests or personal relationships that could have appeared to influence the work reported in this paper.

☐The authors declare the following financial interests/personal relationships which may be considered as potential competing interests:

***Author Contributions Section**

Vimala Devi Mohan and Liji Sobhana. S. S contributed to the experimental design, synthesis and preparation of LDH and writing the manuscript. Vimala Devi and Punalur John Shiny contributed to the Preparation of scaffolds, *In vitro* characterization and Histopathology interpretation of the nanofibrous matrices.Vimala Devi, Punalur John Shiny, Giriprasath Ramanathan and Grace Felciya Sekar Jeyakumar contributed to the design of *in vivo* experiments and their data acquisition and analysis. Velswamy Poornima contributed in the data analysis and interpretation, and manuscript writing. Pedro Fardim, Sathiah Thennarasu, and Uma Tiruchirapalli Sivagnanam were contributed to the overall cconception and design of the work , Evaluating results, Assisting in interpretation of data in writing manuscript and overall responsibility.